UNIVERSITAT ROVIRA I VIRGILI
TRANSPORTE NO PASIVO DE COMPUESTOS ORGÁNICOS VOLÁTILES EN LA ZONA NO SATURADA.
Orlando Silva Rojas
ISBN: 978-84-690-7612-5 / DL: T.1217-2007

# Non-Passive Transport of Volatile Organic Compounds Infiltrated from a Soil-Surface Disk Source

Orlando Silva and Jordi Grifoll*

Grup de Recerca de Fenòmens de Transport
Departament d'Enginyeria Quimica,
Universitat Rovira i Virgili,
Av. dels Països Catalans 26,
43007 Tarragona, Spain.

*Corresponding author. Tel.: +34 977 55 96 39; fax +34 977 55 96 21
*E-mail addresses*:
orlando.silva@urv.cat (O. Silva), jordi.grifoll@urv.cat (J. Grifoll)

**Abstract**

The presence of some chemicals in the vadose zone can affect the physical properties of the fluid phases leading to transport processes known as non-passive. Common numerical models do not account for the simultaneous interaction of various non-passive effects on unsaturated flow and transport. The unsaturated flow and non-passive transport model for water-soluble organic compounds previously developed by Silva and Grifoll (2007), was implemented in cylindrical coordinates with a top boundary condition that accounts for different zones of the surface to simultaneously be under infiltration or volatilization. The model was applied to the simulation of two-dimensional infiltration of aqueous mixtures of methanol from a disk source, its redistribution and volatilization in both homogeneous and heterogeneous soils. Simulations showed that methanol concentration significantly affects volumetric liquid content and concentration profiles, as well as the fraction of infiltrated mass of methanol that is released to the atmosphere. Concentration-dependent viscosity had the major impact on the liquid flow, and acted in the same or opposite direction of surface tension effects, depending on the composition and the magnitude of the concentration gradients developed in the soil. Heterogeneity favored the non-passivity as the differences in volumetric liquid content and normalized concentration of methanol became more pronounced during the transport through a soil composed by a clay lens embedded within a main matrix of sandy clay loam texture. Dispersion in the liquid-phase was the predominant mechanism that globally drives the methanol transport when dispersivity at saturation was set to 7.8 cm. However, for a dispersivity at saturation set to 1.0 cm, changes in surface tension due to variation in composition induced significantly higher liquid flow and convection in the liquid-phase was the most active transport mechanism, for homogeneous soils and highly concentrated infiltrating mixtures. On the contrary, since the clay lens and a higher drying of the surface dispersed the concentration gradients above the lens, for the heterogeneous soil experiment with a lower dispersivity liquid-phase dispersion was again the dominant transport mechanism.

UNIVERSITAT ROVIRA I VIRGILI
TRANSPORTE NO PASIVO DE COMPUESTOS ORGÁNICOS VOLÁTILES EN LA ZONA NO SATURADA.
Orlando Silva Rojas
ISBN: 978-84-690-7612-5 / DL: T.1217-2007

## 1. Introduction

It is common in numerical models of flow and transport through the vadose zone to assume that flow and solute transport do not depend on composition (Grifoll and Cohen, 1996). Often this assumption is considered in order to simplify calculations, because with no concentration-dependent transport properties the governing equations are solved in an uncoupled fashion. However, some chemicals could be present in water at concentrations that affect the physical properties of the liquid and gas phases. Under this condition, the coupled transport of fluid phases and chemicals through the unsaturated zone becomes a highly interactive phenomenon, where matric pressure gradients can induce solute transport and, reciprocally, the mixture composition may change the transport properties and induce a given pattern of flow. The resulting transport processes are known as non-passive (Silva and Grifoll, 2007). Therefore, modeling of infiltration, redistribution and volatilization/evaporation of such aqueous mixtures should take into consideration their non-passive behavior.

Most of the previous research regarding non-passive transport through the vadose zone has mainly been focused on the dependence of a few properties (density, viscosity or surface tension) on composition (e.g. Boufadel et al., 1997, 1999; Smith and Gillham, 1994, 1999; Ouyang and Zheng, 1999). Often the tendency in these works has been to study separately the effects of each concentration-dependent properties on mass transport and flow. Systems that can exhibit non-passive transport include saline solutions (Boufadel et al., 1997, 1999; Weisbrod et al., 2004; Zhang et al., 2005), organic compounds as oxygenate gasoline additives (Ferreira et al., 2001; Da Silva and Alvarez, 2002; Deeb et al., 2002; McDowell and Powers, 2003), some pesticides (Ouyang and Zheng, 1999) and surfactant dissolutions (Smith and Gillham, 1994, 1999; Henry et al. 1999, 2001, 2002; Henry and Smith, 2002; Henry and Smith, 2006).

Although there are a number of numerical models that can be adapted to simulate some situations of non-passive solute transport through the vadose zone in multiphase systems, (e.g., STOMP, White and Oostrom, 2000; VST2D, Friedel, 2000), in most of them it is assumed that several properties are independent of the mixture composition. Recently, Silva and Grifoll (2007) formulated a detailed model to describe the non-passive transport of water-soluble chemicals in the unsaturated zone and used it to illustrate the infiltration and redistribution of alcohol-water mixtures. On the basis of previous studies about non-passive transport, already referenced in Silva and Grifoll (2007), these authors developed their model



that includes the dependence of density, viscosity, surface tension, molecular diffusion coefficient in the liquid phase, and gas-liquid partition coefficient on the aqueous mixture composition. The decrease in the gas-liquid partition coefficient at high capillary pressures was considered in accordance with Kelvin's equation for multi-component mixtures. One-dimensional (1D) simulations of methanol infiltration and redistribution in two different soils showed that the mixture composition significantly affects volumetric liquid content and concentration profiles, as well as the volatilization of the aqueous mixture.

Regardless of the usefulness of 1D modeling of solute transport and flow in the vadose zone, this approach is not capable of describing some phenomena that are inherent to the soil three-dimensional nature. There is no doubt that some systems and flow processes require a two-dimensional (2D) modeling approach (see e.g., Smith and Gillham, 1999; Henry and Smith, 2002; Henry et al., 2002; Henry and Smith, 2006). Particularly, multidimensional modeling may be more suitable in heterogeneous systems because they involve some characteristics that, excepting the case of uniform layered soils, can not be captured by 1D simulations. Some experimental and modeling studies have focused on the 2D transport of volatile organic compound through homogeneous soils, with non-passivity given by a dependence of density, viscosity and/or surface tension on composition (Ouyang and Zheng, 1999; Henry and Smith, 2002; Henry et al., 2002; Weisbrod et al., 2004; Henry and Smith, 2006). On the other hand, non-passive transport of some substances through heterogeneous soils may show coupling of mechanisms or processes that would not occur in homogeneous media. There are several studies showing the effect of porous medium heterogeneities on 2D flow and transport in the vadose zone (Pan and Wieranga, 1997; Walker et al., 1998; Wang and Feyen, 1998; Hofstee et al., 1998; Wildenschild and Jensen, 1999a, 1999b; Oostrom et al., 2003; Weisbrod et al., 2003; Taylor et al., 2004; Robert et al., 2006). Various of these works deal with the case of NAPL transport, including the effects of the surfactant addition, in soils composed by a main matrix containing one or more lenses of different textural class (Hofstee et al., 1998; Schroth et al., 1998; Walker et al., 1998; Rathfelder et al., 2001; Taylor et al., 2001; Ramsburg and Pennel, 2002; Oostrom et al., 2003; Ramsburg et al., 2004; Taylor et al., 2004). For instance, the work of Taylor et al. (2004) investigated the influence of ethanol concentration on the aqueous flow field and tetrachloroethene (PCE) mass recovery through a combination of numerical simulations and experiments, including 2D geometries. These experiments were conducted in a sand box to quantify the effects of ethanol addition to a nonionic surfactant solution (4% Tween 80) on PCE solubilization rate and capacity,

UNIVERSITAT ROVIRA I VIRGILI
TRANSPORTE NO PASIVO DE COMPUESTOS ORGÁNICOS VOLÁTILES EN LA ZONA NO SATURADA.
Orlando Silva Rojas
ISBN: 978-84-690-7612-5 / DL: T.1217-2007

relevant solution properties, flushing solution delivery, and contaminant recovery. Density and viscosity dependent concentration relationships were incorporated into a numerical model (Rathfelder et al., 2001) to simulate fluid flow and DNAPL recovery. Results showed that small differences between flushing and resident solution density can strongly influence surfactant front propagation. Comparison between measured and predicted results indicated that accurate simulation of PCE recovery using ethanol amended flushing solution depended on coupled effects of mass transfer limitations, subsurface layering and solution density contrast.

Though there are in the literature some studies that deal with the modeling of 2D density-, viscosity- and/or surface tension- dependent flow (Ouyang and Zheng, 1999; Rathfelder et al., 2001; Rathfelder et al., 2001; Henry et al., 2002; Henry and Smith, 2006), there is a lack of studies about 2D simulations of non-passive transport of volatile organic compounds in the vadose zone, with several concentration-dependent transport properties. In particular, excepting the work of Henry and Smith (2006), there are not experimental or numerical researches regarding with the non-passive transport effects on infiltration from a line or disk source. Additionally, in modeling studies non flow boundary conditions are often specified on the soil surface instead of volatilization/evaporation boundary conditions, because the lesser complexity associated in the numerical resolution. However, the combination of infiltration from a line or disk source and volatilization boundary conditions at the soil surface provides a more realistic description of the physical processes that occur, for instance, in spills at field scale. Accordingly, in the present work we apply the unsaturated flow and non-passive transport model for water-soluble organic compounds previously developed by Silva and Grifoll (2007), to simulate the infiltration of methanol-water mixtures from a disk source both into 2D homogeneous and heterogeneous soils, its redistribution within the soil and volatilization to the atmosphere.

## 2. Basic equations and numerical resolution

The detailed equations of the non-passive transport model used in this work and the details of its implementation in a one-dimensional system are given elsewhere (Silva and Grifoll, 2007). A brief description of the main features of the model and the implementation details in two-dimensional cylindrical coordinate system ($r$, $z$) are given below.



### *2.1. Balance equations*

The unsaturated soil system considered consists of liquid ($l$), gas ($g$) and solid ($s$) phases. Components that may be present within these phases are water, dry-air and $N-2$ water-soluble organic compounds. Inter-phase mass transfer is modeled assuming local phase equilibrium. The mass-conservation equation for component $k$ under isothermal conditions is given by (Silva and Grifoll, 2007)

$$\frac{\partial \varphi_k C_l^k}{\partial t} = -\nabla \cdot \left( \mathbf{J_l^k} + \mathbf{J_g^k} + \boldsymbol{\beta}_\mathbf{k} C_l^k \right) \tag{1a}$$

$$\varphi_k = \theta_l + \theta_g H_{gl}^k + \theta_s H_{sl}^k \tag{1b}$$

$$\boldsymbol{\beta}_\mathbf{k} = \mathbf{q_l} + \mathbf{q_g} H_{gl}^k \tag{1c}$$

where $C_i^k$ (kg/m$^3$) is the concentration of component $k$ ($k$ = 1,...,$N$) in the phase $i$ ($i$ = $l$, $g$, $s$), $\theta_i$ (m$^3$/m$^3$) is the volumetric fraction of that phase, $\mathbf{q_i}$ (m/s) is the specific discharge of the fluid phase $i$, and $H_{ij}^k = C_i^k / C_j^k$ are the partition coefficients for component $k$ between phases $i$ and $j$. The specific discharge of phase $i$, $\mathbf{q_i}$, is given by the generalized Darcy's law (Bear and Bachmat, 1991)

$$\mathbf{q_i} = -\frac{\mathbf{k} k_{ri}}{\mu_i} \left( \nabla P_i + \rho_i g \mathbf{e_z} \right) \tag{2}$$

In Eq. (2), $\mathbf{k}$ is the intrinsic permeability tensor of the soil (m$^2$), $g$ (m/s$^2$) is the acceleration of gravity, $\mathbf{e_z}$ is a unit vector in the vertical direction (positive upwards), $k_{ri}$ is the relative permeability (dimensionless), $\rho_i$ (kg/m$^3$) is the density, $\mu_i$ (kg/m-s) is the dynamic viscosity, and $P_i$ (Pa) is the pressure of the phase $i$. The diffusive-dispersive mass flux vector $\mathbf{J_i^k}$ (kg/m$^2$-s) is given by

$$\mathbf{J_i^k} = -\theta_i \mathbf{D_i^k} \nabla C_i^k \tag{3}$$

UNIVERSITAT ROVIRA I VIRGILI
TRANSPORTE NO PASIVO DE COMPUESTOS ORGÁNICOS VOLÁTILES EN LA ZONA NO SATURADA.
Orlando Silva Rojas
ISBN: 978-84-690-7612-5 / DL: T.1217-2007

where $\mathbf{D_i^k}$ ($m^2/s$) is the diffusion-dispersion tensor for component *k* in the phase *i* (Bear and Bachmat, 1991). Assuming that dry-air is present neither in the liquid- nor in the solid-phases, only the gas-phase transport was considered for the dry-air mass conservation equation

$$\frac{\partial \theta_g C_g^a}{\partial t} = -\nabla \cdot \left[ \mathbf{J_g^a} + \mathbf{q_g} C_g^a \right] \tag{4}$$

where $C_g^a$ is the dry air concentration in the gas-phase. The diffusive-dispersive mass flux vectors of air in the gas-phase, $\mathbf{J_g^a}$ ($kg/m^2$-s), and water in the liquid-phase, $\mathbf{J_l^w}$ ($kg/m^2$-s), were calculated from the condition of zero sum of diffusive-dispersive mass fluxes of all components in each fluid phase

$$\mathbf{J_g^a} = -\sum_{k=1,k\neq a}^{N} \mathbf{J_g^k} \tag{5a}$$

$$\mathbf{J_l^w} = -\sum_{k=1,k\neq a,w}^{N} \mathbf{J_l^k} \tag{5b}$$

It is very common when modeling solute transport in variably-saturated soils to assume the condition of constant partition coefficients. Nevertheless, some authors have provided general thermodynamic-based relationships describing the gas-liquid equilibrium for multicomponent liquid mixtures in unsaturated soils (Defay et al., 1966; Rowlinson and Widom, 1984; Shapiro and Stenby, 1997), including salt effects on water vapor pressure and liquid pressure for unsaturated soils (Burns et al., 2000a, 2000b). Accordingly, in the present model the gas-liquid partition coefficient, $H_{gl}^k$, is assumed to be dependent on solute concentration and soil-liquid content (Chen et al., 2000; Chen and Rolston, 2000; Silva and Grifoll, 2007) as given by

$$H_{gl}^k = H_{gl}^{*k} \exp\left( \frac{P_M \hat{V}^k}{RT} \right) \tag{6}$$

where the exponential term accounts for the Kelvin's effect in multicomponent liquid mixtures (Defay et al., 1966; Rowlinson and Widom, 1984). In Eq. (6), $\hat{V}^k$ ($m^3$/mol) is the



partial molar volume of component *k* in the liquid-phase, *R* is the universal gas constant, $P_M = P_l - P_g$ (Pa), is the matric pressure of the liquid and *T* (K) the temperature. The gas-liquid partition coefficient for plane interfacial surfaces corresponds to the dimensionless Henry's law constant, $H_{gl}^{*k}$, and its dependence on component concentration was calculated from the liquid-vapor equilibrium condition (Valsaraj, 1995)

$$H_{gl}^{*k} = \gamma^k \frac{p_{vap}^k \hat{V}_m}{RT} \tag{7}$$

in which $p_{vap}^k$ (Pa) is the vapor pressure of component *k*, $\hat{V}_m$ ($m^3$/mol) is the partial molar volume of the liquid mixture, and $\gamma^k$ (dimensionless) is the activity coefficient of component *k*. Matric pressure was defined originally to be applied under the action of capillary forces and not under adsorptive forces. In very dry soils, the small quantity of liquid in the medium is no longer under the influence of capillary forces and then, strictly, the original matric pressure definition is not applicable. However, as Baggio et al. (1997) suggested, matric pressure can be defined as $P_M = -\Delta h / \hat{V}_m$, where $\Delta h$ (J/mol) refers to the enthalpy difference between the vapor in the gas-phase and the condensed and/or adsorbed liquid-phase, excluding the latent enthalpy of vaporization. Taking this definition, matric pressure and Kelvin's equation can be applied all the range of water content from saturation to complete dry conditions (Gawin et al., 2002; Schrefler, 2004).

*2.2. System description and boundary conditions*

The 2D version of the non-passive transport model described previously was implemented in cylindrical coordinates and used to simulate the infiltration, redistribution and volatilization/evaporation of methanol-water mixtures in unsaturated soils. The 2D domain considered in the simulations is shown in Fig.1. When imposing boundary conditions at the soil surface, two zones were distinguished: zone A and zone B. Zone A, which extends from $r = 0$ to $r = r_c$, is a disk source infiltration zone where a constant liquid infiltration flux, $q_{l0}$ (m/s), is imposed from $t = 0$ to $t = t_c$, followed by evaporation/volatilization for $t > t_c$. In zone B, which extends from $r = r_c$ to $r = R_0$, evaporation/volatilization is allowed along the all simulation.

UNIVERSITAT ROVIRA I VIRGILI
TRANSPORTE NO PASIVO DE COMPUESTOS ORGÁNICOS VOLÁTILES EN LA ZONA NO SATURADA.
Orlando Silva Rojas
ISBN: 978-84-690-7612-5 / DL: T.1217-2007

When zone A was under infiltration, the top boundary condition for transport of each component *k*, in this zone (Eq. (1)) was the component mass flux in the *z*-direction at the surface, $N_0^k$ (kg/m$^2$ s), calculated as

$$N_0^k = q_{l0} C_{l,\text{in}}^k \tag{8}$$

where $C_{l,\text{in}}^k$ (kg/m$^3$) is the given concentration of component *k* in the infiltrating liquid. In zone B and for $t > t_c$ in zone A, the evaporation/volatilization mass flux for component *k* at the surface was calculated considering a mass transfer limitation from the soil surface to the bulk atmosphere (Brutsaert, 1975; Grifoll and Cohen, 1996)

$$N_0^k = k_0^k \left( C_b^k - C_{g0}^k \right) \tag{9}$$

In Eq. (9), $k_0^k$ (m/s) is the atmosphere-side mass transfer coefficient for component *k*, $C_b^k$ (kg/m$^3$) is the background concentration of component *k* in the atmosphere, and $C_{g0}^k$ (kg/m$^3$) is the concentration of component *k* in the gas-phase at the soil surface. For given values of wind velocity, soil roughness and Schmidt number of the chemical volatilized, the mass transfer coefficients, $k_0^k$, were estimated with the semi-empirical correlation proposed by Brutsaert (1975) developed for neutral atmospheric conditions. In all cases the boundary condition at the bottom, $z = L$, was set as zero diffusive and dispersive fluxes and zero matric pressure gradient. Also it was assumed zero radial fluxes at the lateral boundary. The lower gas-phase boundary condition was set as a no-flow boundary while the upper gas-phase boundary condition was a constant atmospheric pressure.

*2.3. Dispersivities, soil-water retention curve and physico-chemical properties*

The diffusion-dispersion tensor for component *k* in the phase *i*, $\mathbf{D_i^k}$ (m$^2$/s), was calculated as

$$\left(\mathbf{D_i^k}\right)_{xy} = \left( \frac{D_{0i}^k}{\tau_i} + \alpha_{Ti} \frac{\|\mathbf{q_i}\|}{\theta_i} \right) \delta_{xy} + \left(\alpha_{Li} - \alpha_{Ti}\right) \frac{q_{xi} q_{yi}}{\theta_i \|\mathbf{q_i}\|} \qquad x, y = z, r \tag{10}$$



where $q_{zi}$ and $q_{ri}$ (m/s) are the axial and radial components of the *i*-phase specific discharge, $\|\mathbf{q_i}\|$ is the magnitude of this flux, $\alpha_{Li}$ and $\alpha_{Ti}$ (m) are the longitudinal and transversal dispersivities, $\delta_{xy}$ is the delta Kronecker function, $D_{0i}^k$ (m$^2$/s) denotes the molecular diffusion coefficient in the phase *i*, and $\tau_i$ (dimensionless) is the tortuosity of phase *i*. Tortuosities, $\tau_g$ and $\tau_l$, were evaluated according to the first model of Millington and Quirk as suggested by Jin and Jury (1996), i.e. $\tau_i = \varepsilon^{2/3}/\theta_i$, where $\varepsilon$ is the soil porosity. In any phase it was assumed transversal dispersivity to be 10% of the longitudinal dispersivity. This longitudinal dispersivity is calculated as a function of the volumetric phase content, in accordance with the correlation proposed by Grifoll et al. (2005)

$$\alpha_{Li} = \alpha_{Li}^o \left(13.6 - 16 S_i + 3.4 S_i^5\right) \tag{11}$$

in which $S_i = \theta_i/\varepsilon$ is the actual saturation of phase *i* and $\alpha_{Li}^o$ is the longitudinal dispersivity at saturation. Grifoll and Cohen (1996) used a similar approach to Eq. (11). Although the empirical longitudinal dispersivity model represented by Eq. (11) is not of general applicability, it has been adopted here to illustrate a general trend of dispersivity behavior (Grifoll and Cohen, 1996). The calculation of dispersivities according Eq. (11) requires the value of dispersivity at saturation, $\alpha_{Li}^o$. In this work, we assumed $\alpha_{Li}^o$ = 7.8 cm for both the liquid and the gas phases, value suggested by Biggar and Nielsen (1976) for saturated soil conditions in an agricultural field (Nielsen and Biggar, 1973). Note that in their work, Nielsen and Biggar (1973) measured dispersivities in ponded soils of several textures (loam, clay loam, silty clay, silty clay loam) under steady state infiltration conditions at depths between 30.5 and 182.9 cm, infiltration pore velocities between 1.3 and 105.4 cm/day, while hydraulic conductivities at saturation ranged from 0.3 to 70 cm/day. In the simulations of the present work, the selected soils and process conditions were, most of the time, within the range of values above described.

1D simulations of transport of methanol-water mixtures in homogeneous soils carried out by Silva and Grifoll (2007) showed that, at least close to the soil surface where volatilization and evaporation occur, the soil may reach levels of very low water content ($\theta_l < 0.10$). More severe dryness conditions are expected for the 2D case. Therefore, to simulate these situations realistically the model includes an extended version of the Brooks-

UNIVERSITAT ROVIRA I VIRGILI
TRANSPORTE NO PASIVO DE COMPUESTOS ORGÁNICOS VOLÁTILES EN LA ZONA NO SATURADA.
Orlando Silva Rojas
ISBN: 978-84-690-7612-5 / DL: T.1217-2007

Corey (BC) soil-water retention curve proposed by Rossi and Nimmo (1994) (RN), which is given as

$$P_{M,w}(S_l) = \begin{cases} P_d e^{-S_l/\alpha_{RN}} & ; \quad 0 \le S_l < S_{lj} \\ P_b S_e^{-1/\lambda} & ; \quad S_{lj} \le S_l \le 1 \end{cases} \tag{12}$$

where $P_{M,w}$ (Pa) is the matric water pressure and $S_e = (S_l - S_{lr})/(1 - S_{lr})$ is the effective liquid saturation, while $P_b$ (Pa) (bubble or air-entry pressure), $\lambda$ (pore size distribution index), and $\theta_{lr}$ ($S_{lr} = \theta_{lr}/\varepsilon$) (residual volumetric water content) are the classical BC parameters. The oven dry matric water pressure, $P_d$, was taken as 980 MPa, as suggested by Rossi and Nimmo (1994). The parameters $\alpha_{RN}$ and $\theta_{lj}$ ($S_{lj} = \theta_{lj}/\varepsilon$), introduced by these authors, were computed as functions of the classical BC parameters, following the method proposed by Morel-Seytoux and Nimmo (1999). Liquid-phase relative permeability was calculated as a function of liquid saturation from the soil-water retention curve and the model of Burdine (1953)

$$k_{rl} = S_l^2 \frac{I(S_l)}{I(1)} \tag{13}$$

where the integral function $I(S_l)$ is given as

$$I(S_l) = \begin{cases} \dfrac{\alpha_{RN}}{2P_d^2}\left(e^{2S_l/\alpha_{RN}} - 1\right) & ; \quad 0 \le S_l < S_{lj} \\ \dfrac{\alpha_{RN}}{2P_d^2}\left(e^{2S_{lj}/\alpha_{RN}} - 1\right) + \dfrac{\lambda}{\lambda+2}\dfrac{(1-S_{lr})}{P_b^2}\left(S_e^{1+2/\lambda} - S_{ej}^{1+2/\lambda}\right) & ; \quad S_{lj} \le S_l \le 1 \end{cases} \tag{14}$$

Given a volumetric liquid content, the matric pressure for pure water as given by Eq. (14) has been scaled for mixtures of composition $C_l^m$ as (Leverett, 1941)

$$P_M = \frac{\sigma(C_l^m)}{\sigma_w} P_{M,w} \tag{15}$$



where $\sigma_w$ (N/m) is the surface tension of water and $\sigma(C_l^m)$ (N/m) is the surface tension of the liquid mixture.

The assumption of non-passive transport implies that some physical properties of the methanol-water mixtures depend on composition. The dependencies of surface tension, liquid density, liquid viscosity and liquid diffusion coefficient on methanol concentration have been described by a polynomial function as given by Silva and Grifoll (2007). On the other hand, diffusion coefficients of methanol and water in the gas-phase were taken as constants, with values $D_{0g}{}^m = 1.6\times10^{-5}$ m$^2$/s (Grifoll and Cohen, 1996) and $D_{0g}{}^w = 2.6\times10^{-5}$ m$^2$/s (Reid et al., 1987), respectively.

Partial molar volumes and the activity coefficients, according to Eqs. (6) and (7), are required to calculate the gas-liquid partition coefficients for methanol and water. Activity coefficients for water and methanol were calculated using Wilson's equation (Kyle, 1999) with the parameters suggested by Gmehling et al. (1988). Molar volumes were calculated following the procedure described by Lide and Kihiaian (1994), who suggested the Redlich-Kister equation to calculate molar excess volumes. The gas-liquid partition coefficient of water, $H_{gl}{}^{w*}$, increases monotonically from $1.73\text{x}10^{-5}$, in absence of methanol, to the limiting value $6.14\text{x}10^{-5}$ as the pure methanol condition is approached. The partition coefficient for methanol, $H_{gl}{}^{m*}$, reaches a minimum value of $1.61\text{x}10^{-4}$ when $C_l^m = 405$ kg/m$^3$ and then increases progressively to $2.17\text{x}10^{-4}$, which is the value for pure methanol. Adsorption of methanol onto the soil-solid phase was assumed to be described by a constant partition coefficient $H_{sl}{}^m = 3.7\text{x}10^{-3}$, estimated for a soil with 2% of organic matter (Grifoll and Cohen, 1996).

*2.4. Numerical procedure*

The governing partial differential equations, Eqs. (1) and (4), were discretized spatially and temporally in algebraic form using the finite volumes method (Patankar, 1980) with a fully implicit scheme for time integration. The non-linear discretized governing equations were solved using the multivariable Newton-Raphson iteration technique (Kelley, 1995). Volumetric liquid content, dry-air concentration in the gas-phase and the methanol concentration in the liquid-phase were selected as primary variables. The Jacobian coefficient matrix was approximated using a finite difference approximation (Kelley, 1995). The linear system of equations formulated in the Newton-Raphson method was solved for the correction

UNIVERSITAT ROVIRA I VIRGILI
TRANSPORTE NO PASIVO DE COMPUESTOS ORGÁNICOS VOLÁTILES EN LA ZONA NO SATURADA.
Orlando Silva Rojas
ISBN: 978-84-690-7612-5 / DL: T.1217-2007

to the primary variables by the iterative Preconditioned Biconjugate Gradient Method (Press et al., 1992; Kelley, 1995). The preconditioner matrix was the diagonal part of the Jacobian coefficient matrix (Press et al., 1992). Values for the convergence criterion and maximum number of Newton-Raphson have been defined conveniently as input parameters. The convergence criterion was defined respect to the maximum residual of each mass balance equation, normalized by the sum of the mass fluxes absolute values. The tolerance employed in all simulations was $10^{-7}$ while the maximum number of Newton-Raphson iterations was set to 50. If the convergence limit was not satisfied after 50 iterations, the time step was reduced to 50% and the calculation was restarted from the end of the previous time step. Otherwise, if the convergence was attained within the maximum number of iterations, the time step was doubled without exceeding a maximum $\Delta t_{max}$ = 120 s, and a new time step was initiated.

A $L$ = 0.5 m, $R_0$ = 0.5 m domain was discretized using a uniform 0.005 m cell spacing in the $z$-direction and a uniform 0.0116 m cell spacing in the $r$-direction, resulting in $N_z$x$N_r$ = 100x43 = 4300 cells. The sensitivity of the numerical solution to grid spacing and time step was analyzed for Test case 1 as it is described in section 3.1 below. For the standard grid and maximum time step, as given above, maximum discrepancies between the numerical results and the exact values are expected to be less than 0.2% in volumetric liquid content and less than 2% in methanol concentration.

To check the numerical algorithm, we simulated the infiltration, redistribution and volatilization of an aqueous mixture of methanol into a sandy clay loam soil, mimicking a 1D situation by fixing the same top boundary condition along the entire surface. The results from this simulation were compared with the 1D non-passive transport solution reported by Silva and Grifoll (2007) with a maximum discrepancy less than 1%. Also, the rapid infiltration of water into a two-dimensional cylindrical system of loamy sand described in Gastó et al. (2002) was reproduced and compared with their fine grid solution giving a discrepancy less than 0.5%.

## 3. Results and Discussion

The impact of the non-passive behavior on the infiltration and redistribution of methanol-water mixtures in two-dimensional systems is illustrated in two test cases in which different soils were used. For every test, three numerical experiments were performed, each one with different methanol concentration in the infiltrating mixture. These concentrations



were chosen as 5, 50 and 90% w/w to cover the range of $C^m_{l,\text{in}}$ from dilute to highly concentrated mixtures.

The first test case was for the infiltration into a homogeneous sandy clay loam soil (Fig. 2a). In the second test case, the soil was assumed to be heterogeneous and composed by a cylindrical block of clay texture embedded within a coarser matrix of sandy clay loam soil texture, as shown in Fig. 2b.

Test 1D simulations previously reported by Silva and Grifoll (2007) showed that the convective gas-phase component did not contribute effectively to the transport of methanol and water in sandy clay loam and silty clay soils and increased the simulation time significantly. Therefore, the results presented in the next sections were obtained by neglecting gas-phase advection when solving the numerical model.

Both in homogeneous and heterogeneous experiments, the upper boundary condition for a first period of $t_c$ = 72 hours was set as an infiltration rate of $q_{l0}$ = 0.3 cm/h in zone A ($r_c$ = 0.1 m) and volatilization in zone B (see Fig. 1), followed by 96 hours in which the methanol and water were allowed to volatilize in both zones (Eq. (10)). The background concentration of methanol in the atmosphere was assumed to be zero, while the background concentration of water in the atmosphere was calculated assuming a constant relative humidity of 40%. The initial conditions were a uniform volumetric water content of 0.128 $m^3/m^3$ and zero methanol concentration throughout the domain. This volumetric water content was attained by fixing a matric potential of –100 m in the sandy clay loam main matrix and –1490 m in the clay lens (see Fig. 2). These values were calculated using the hydraulic parameters for Eqs. (13), (14) and (15), taken from Rawls and Brakensiek (1989) as typical values for sandy clay loam and clay soils, which are given in Table 1.

### *3.1. Test case 1: Homogeneous soil*

The first case study involved three simulations of the infiltration of a methanol-water mixture into a homogeneous sandy clay loam soil (Fig. 2a), each one with different methanol concentration of the infiltrating liquid, $C^m_{l,\text{in}}$ = 39.3 kg/$m^3$ (5% w/w), 393.3 kg/$m^3$ (50% w/w) and 707.9 kg/$m^3$ (90% w/w).

UNIVERSITAT ROVIRA I VIRGILI
TRANSPORTE NO PASIVO DE COMPUESTOS ORGÁNICOS VOLÁTILES EN LA ZONA NO SATURADA.
Orlando Silva Rojas
ISBN: 978-84-690-7612-5 / DL: T.1217-2007

Sensibility of the numerical solution to the grid size and time step

Six simulations with different grids were run for a maximum time step of $\Delta t_{max}$ = 120 s and the mixture at 90% w/w for which more noticeable non-passive effects are expected. One of these simulations corresponds to the selected grid that was described in the section 2.4, and that involved $N_z$x$N_r$ = 100x43 cells. The other five simulations were run also with uniform grids constructed by halving or doubling the grid spacing in the radial and axial directions. These grids involved $N_z$x$N_r$ = 25x43, 33x43, 50x43, 25x86 and 50x86 cells, which gives two sets of simulations for *z*-direction grid spacing analysis and also two sets of simulations for *r*-direction grid spacing analysis. The latter showed insignificant variation of the results to *r*-direction grid spacing. For axial grid spacing analysis, as observed by Silva and Grifoll (2007) in the 1D non-passive transport of methanol-water mixtures in unsaturated soils, here it also was found that, at the end of simulation ($t$ = 168 h), the major discrepancies in volumetric liquid content and concentration were localized along the soil surface (zone A). The volumetric liquid content and methanol concentration at the surface, both at $r = 0$ and $r = r_c$, obtained at the end of the simulations were extrapolated to an infinite number of control volumes, $\theta_{l0}^{\infty}$ and $C_{l0}^{\infty}$. This was accomplished using the results data available for $N_z$ = 25, 34, 50 and 100 and a constant $N_r$ = 43. Fig. 3 shows the ratio of $\theta_{l0}$ and $C_{l0}$ to their extrapolated value $\theta_{l0}^{\infty}$ and $C_{l0}^{\infty}$ as a function of the inverse of the number of control volumes, $1/N_z$. Deviations from the extrapolated volumetric liquid content for the selected grid ($N_z$ = 100) were less than 0.2% (Fig. 3a). Deviations were higher in the case of methanol concentration. However, for the selected grid, the relative deviation was less than 2% (Fig. 3b). In addition, two simulations were run using maximum time steps of 30 and 60 s, but the differences in $C_{l0}$ respect the results for $\Delta t_{max}$ = 120 s were also less than 2%, indicating that the selection of this maximum time step was appropriate.

Flow and redistribution of the liquid mixture

Fig. 4 shows the volumetric liquid content (Fig. 4a-c) and the normalized concentration (Fig. 4d-f) profiles at the end of the simulation ($t$ = 168 h) for the three infiltrating mixtures. Normalization of concentration has been carried out with respect $C_{l,\mathrm{in}}^{m}$ in order to emphasize the non-passive behavior. In case of passive transport, the normalized concentration profiles in Fig. 4d-f should be independent of concentration and would coincide



in a unique figure because the solute transport equation (Eq. (1)) is linear when the coefficients do not depend on the solute concentration (Silva and Grifoll, 2007).

For the present non-passive transport simulations, the different infiltrating aqueous mixtures of methanol evolve towards a different distribution of liquid-phase and normalized concentration, which makes clear the deviations one can expect when the dependency of physical properties on composition are not taken into account. As shown in Fig. 4a-c, at the end of the simulations ($t$ = 168 h) relative significant differences in volumetric liquid content have been developed in the region of center of mass of the profile, or "blob" region, around $z$ = 0.2 m. Also, small differences are observed both in the region close to the surface and in the liquid front advance. Silva and Grifoll (2007) found that the differences in volumetric liquid content profiles for different $C_{l,\mathrm{in}}^{m}$, are caused by a combination of three factors: i) the dilution effect on the incoming mixture caused by the initial pure water in the soil, ii) differences in the liquid-phase flow caused by changes in viscosity, density and surface tension, and iii) the volatilization of the mixture.

First, we note that the specific gravity of the mixture changes monotonically from 1.0 for pure water to 0.786 for pure methanol. Then, when methanol dilutes in water, the volume of the mixture shrinks because the non-ideal mixing effect (Silva and Grifoll, 2007). The non-additivity of volumes principle and the density concentration-dependent relationship implies that the non-ideal mixing effect, calculated as percentage of the infiltrated liquid volume that vanishes due to the non-ideality, cannot exceed a 3.8% for any aqueous mixture of methanol. On the other hand, the volatilized volume of liquid was calculated by integration of the volatilization/evaporation fluxes given by Eq. (9), divided by the density of the mixture at surface. In order to make comparisons between the different $C_{l,\mathrm{in}}^{m}$ cases that are independent of the domain size, it is convenient to subtract from the volatilized volume of liquid the volume of water that evaporates in absence of infiltration. This difference, expressed as percentage of the infiltrated volume of liquid was 38.8%, 31.1% and 34.1% for 5%, 50% and 90% w/w mixtures, respectively. These percentages seem to be inconsistent with the degree of drying of the top soil observed in Fig. 4a-c, where it is apparent that the infiltration of the 90% w/w mixture led to a higher drying in this zone. However, they result from a combination of the volatilization/evaporation fluxes (Eq. (9)) and the effect of concentration-dependent viscosity on the liquid flow. First, it was found that more than the half of the volatilized volume of liquid was released to the atmosphere during the infiltration period (first 72 hours), and this amount was higher for more concentrated infiltrating mixtures. During this

UNIVERSITAT ROVIRA I VIRGILI
TRANSPORTE NO PASIVO DE COMPUESTOS ORGÁNICOS VOLÁTILES EN LA ZONA NO SATURADA.
Orlando Silva Rojas
ISBN: 978-84-690-7612-5 / DL: T.1217-2007

period, the intermediate and more concentrated mixtures flow more slowly because its higher viscosity, and consequently, by remaining close to the surface for a longer period, undergo a higher volatilization near $r = r_c$ within zone B. Secondly, the volume of the liquid volatilized after infiltration (next 96 hours) was lower for the more concentrated mixture due mainly to viscosity effects. Once the top-soil became enough dry on the zone A after infiltration, because its higher viscosity, the more concentrated mixture cannot flow upward as faster as the more dilute mixture do. The liquid-phase transport of water and methanol from inside to the surface is reduced in this zone. Consequently, because the volatilization rate at the surface is low for low concentrations of methanol and the evaporation rate is low for low concentrations of water, the volume of volatilized liquid decreases.

Figures 4a-c also show that the "blob" region with relatively high liquid content ($0.15 < \theta_l < 0.17$), located approximately at 2-cm depth, increases and becomes shallower as the infiltrating mixture was more concentrated in methanol. These differences in behavior are the consequence of the dependence of dynamic viscosity on concentration. To illustrate the effect of viscosity in these different experiments, Fig. 5 shows the contour plot of the liquid-phase dynamic viscosity for the three experiments normalized respect the viscosity of pure water. It is apparent that whereas this viscosity is almost equal to the value for water in all the domain at the end of the first experiment (Fig. 5a), increases appreciably in a small volume around 0.15-m depth in the second experiment (Fig. 5b) and is more than 1.8 times the viscosity of pure water in a large volume that goes from a few centimeters below surface to the depth of 0.15 m in the third experiment (Fig. 5c). In order to show that the concentration-dependent viscosity was the main responsible for the differences in volumetric liquid content depicted in Fig. 4a-c, a new simulation with a constant viscosity and equal to the pure water viscosity was run for the 90% w/w experiment. The liquid content distribution at the end of this experiment is shown in Fig. 6, that should be compared to the volumetric liquid content distribution for non-passive transport (Fig. 4c). As shown in Fig. 6, constant viscosity causes lower local volumetric liquid content, and led to a profile that is similar to the volumetric liquid content profile obtained for concentration-dependent viscosity with a 50% w/w infiltrating mixture (see Fig. 4b) This shows that the increased viscosity at the end of the 90% w/w experiment with concentration-dependent viscosity contributes to maintain the large region of high liquid content depicted in Fig 4c. Although for the more dilute infiltrating mixture the total amount of liquid within the soil was higher, the infiltration of the more concentrated mixture (90% w/w) yields higher local volumetric liquid contents. It is



noteworthy that, for all the mixtures, the location of the maximum liquid content zone (Fig. 4a-c) was below the location of maximum concentration level (Fig. 4d-f). In fact, the distance between these two depths, i.e., between the centers of mass of moisture and concentration profiles, increased from 3.6 cm for the 5% w/w mixture to 7.4 cm for the 90% w/w mixture. One could expect that the higher volumetric liquid contents caused by the infiltration of the more concentrated mixture were due to an increase in the liquid flow induced by a higher reduction in surface tension (Smith and Gillham, 1994, 1999). Nevertheless, Silva and Grifoll (2007) found that for 1D non-passive transport of methanol-water mixtures and a dispersivity of 7.8 cm, the contribution to the matric pressure gradient caused by changes in the composition of the mixture through its impact on surface tension, was small. This further confirms that the main responsible for the higher volumetric liquid contents observed in the 90% w/w case is the effect of a higher viscosity on the hydraulic conductivity (Eq. (2)), which yields a slower liquid flow in both axial and radial directions.

The maximum relative difference in volumetric liquid content established between 5% and 90% w/w profiles was about 155% at $z = 1.25$ cm, $r = 22.2$ cm. Additionally, because of the combined effect of volatilization, viscosity and surface tension dependent flow, and non-ideal mixing, the liquid front position (given by an isovolumetric curve at the initial volumetric liquid content value) for the more dilute mixture (5% w/w) advanced almost 7% more than for the more concentrated one.

Distribution of concentration and transport mechanisms

To analyze the differences shown in Fig. 4d-f, it is important to note first that the gas-liquid partition coefficient for methanol is between 6 and 10 times higher than for water (Silva and Grifoll, 2007). Higher overall volatilization rates are therefore expected for more concentrated mixtures. The differences in the normalized methanol concentration profiles developed at the top soil and near zone A, are largely due to methanol transfer limitations from inside the soil to the surface, which are higher for the more dilute mixture (5% w/w). This is shown in Fig. 4d-f, where we find a large difference between the three concentration profiles established in the first 5 cm adjacent to the soil surface. The maximum relative difference in the normalized methanol concentration between 5% and 90% w/w profiles was about 173% at $z = 2.75$ cm, $r = 29.8$ cm. In their work, Silva and Grifoll (2007) simulated the 1D non-passive transport of aqueous mixtures of methanol in the same soil and similar boundary conditions, finding that for a dispersivity value of 7.8 cm, the predominant

UNIVERSITAT ROVIRA I VIRGILI
TRANSPORTE NO PASIVO DE COMPUESTOS ORGÁNICOS VOLÁTILES EN LA ZONA NO SATURADA.
Orlando Silva Rojas
ISBN: 978-84-690-7612-5 / DL: T.1217-2007

mechanism in the transport of methanol through the soil was dispersion in the liquid-phase, with a major contribution from gas-phase diffusion near the surface during the volatilization period. As expected because the similarity with the 1D non-passive numerical experiment, at $t$ = 168 h, the predominant mechanism in methanol transport in the present 2D homogeneous soil simulations with a saturated dispersivity of 7.8 cm was also dispersion in the liquid-phase. The liquid-phase convection had a little contribution in the transport of the more concentrated infiltrating mixture (90% w/w). Also, the gas-phase diffusion is not an active mechanism for methanol transport, except very close to the soil surface and when the composition of the infiltrating mixture is higher than 50% w/w. In these circumstances the soil close to the surface is very dry (see Fig. 4b-c) and in this region no mechanism in the liquid-phase is able to transport the methanol. Diffusion in the gas-phase is therefore the only active mechanism in this thin region. The methanol concentration gradient that drives the gas-phase diffusion is magnified by the Kelvin effect that decreases the concentration of methanol close to the surface, as the soil becomes drier. In the numerical experiments with 90% w/w and 50% w/w mixtures there were lower liquid saturation close to the surface, which induced higher gas-phase diffusive fluxes. For the 5% w/w mixture, the top soil is less dry because volatilization is lower for lower concentrations of methanol. For this mixture, therefore, dispersion in the liquid-phase was the most active mechanism of methanol transport at the top soil region. Note that the mass fluxes for methanol transport were higher for the more concentrated infiltrating mixture.

Also there were differences in the shape of the normalized plume of methanol, which consist in the formation of a "bump" at a depth coincident with the center of mass of the concentration distribution (between $z$ = 10 cm and $z$ = 15 cm). This bump extends in the radial direction and was much more pronounced with the more concentrated mixture (see Fig. 4f). It has been demonstrated that the more concentrated mixture flowed slower than the other mixture because its higher viscosity. This led to an increase in the amount of methanol near the soil surface that is available for volatilization during the infiltration period. On the other hand, because there were higher concentrations of methanol within the soil in the 90% w/w experiment, and larger concentration gradients, the transport of methanol by dispersion and convection in the liquid-phase in both the axial and radial directions was also higher. Consequently, the "bump" of concentration was formed during the infiltration period as a result of a balance between the mechanisms that transport the liquid and methanol upward, because the volatilization/evaporation processes, and the mechanisms for methanol transport



within the soil. Note that the location of this bump of concentration (around $z$ = 0.1 m and $r$ = 0.3 m, in Fig. 4f) coincided with the location of a "notch" in the liquid content contour lines of the more concentrated infiltrating mixture (see Fig. 4c). A similar notch was experimentally observed in 1D by Allred and Brown (1996a, 1996b) who studied the transport of two types of anionic surfactants in unsaturated columns. They found that the notch coincided with the solute front and concluded that it was caused by a modification in the soil-water retention relationship in the transition zone of the soil between high and low concentrations. Also, through numerical simulations of the 1D non-passive transport of aqueous mixtures of methanol in a sandy clay loam soil, Silva and Grifoll (2007) noted a notch in volumetric liquid content profile just in the solute front position. Hence, Figs. 4c and 4f show that in 2D and for a saturated dispersivity of 7.8 cm, the effects of concentration-dependent changes in surface tension on the liquid retention curve, developed in the transition zone of the soil between high and low concentrations may be important, as long as there are high enough concentrations.

Liquid-phase velocity field

Fig. 7 shows the liquid-phase velocity fields obtained at the end of the simulation for the 3 infiltrating mixtures. The first observation is that liquid flow is higher for the more dilute mixture (5% w/w) and decreases as the concentration of methanol in the infiltrating mixture increases. The extension of the velocity field clearly coincides with the advance of the liquid front (Fig. 4a-c), which was previously defined by an isovolumetric curve at the initial volumetric liquid content value ($\theta_i$ = 0.128 $m^3/m^3$). These significant differences in the liquid flux were mainly due to the different viscosity profiles from different compositions of the infiltrating methanol-water mixture (see Fig. 5). According to Eq (2), higher viscosities reduce the hydraulic conductivity, which yields a slower liquid flow in both axial and radial directions. Secondly, as the methanol concentration of the infiltrating mixture is higher the specific discharge of liquid-phase near the soil surface is smaller. Because the drying of the soil is more severe in this zone when the infiltrated mixture is more concentrated in methanol, the relative hydraulic conductivity will be lower and thus, the liquid-phase flow will be reduced. This results are quite similar to those obtained by Silva and Grifoll (2007) in the 1D case of non-passive transport of methanol-water mixtures in a sandy clay loam soil. In fact, in the present 2D simulations we also found that the contribution to the specific discharge from the gravity flux was negligible and the main contribution was from capillary flux. One could

UNIVERSITAT ROVIRA I VIRGILI
TRANSPORTE NO PASIVO DE COMPUESTOS ORGÁNICOS VOLÁTILES EN LA ZONA NO SATURADA.
Orlando Silva Rojas
ISBN: 978-84-690-7612-5 / DL: T.1217-2007

expect higher liquid-phase velocities for the 90% w/w mixture, because higher concentrations of methanol cause a higher reduction in the capillary pressure (Eq. (16)), which would induce important liquid flow (Smith and Gillham, 1994, 1999). However, as in the 1D case (Silva and Grifoll, 2007), with a saturated dispersivity of 7.8 cm the methanol concentration gradients are very dispersed. This reduced the impact of concentration-dependent surface tension on the liquid-phase velocity field. Therefore, the main flow mechanism for the 2D infiltration of methanol was the capillary component due to variations in liquid content.

It is also important to note the close relationship between the volumetric liquid content and concentration profiles in Fig. 4, the liquid-phase velocities in Fig. 7 and the partial mass fluxes involved in the non-passive transport of methanol. Note that the redistribution of the more concentrated infiltrating mixture resulted in higher viscosities within the soil (Fig. 5). As the viscosity is higher, the velocities are lower (Fig. 7c) and a reduction in the liquid-phase dispersion could be expected for the 90% w/w mixture just above the liquid front position in the different numerical experiments (e.g., $z = 0.4$ m, $r = 0$). However, the higher the infiltrating concentration, the lower the volumetric liquid content and the higher the methanol concentration gradients around this region. This leads to higher dispersive fluxes around this zone for the more concentrated infiltrating mixture. A similar analysis explains the interaction between the liquid-phase velocity, the different transport mechanisms and the liquid content and concentration profiles in the upper part of the soil ($z \leq 0.15$ m).

Methanol volatilization

As discussed above, the non-passivity in transport of methanol-water mixtures affected the volume of liquid volatilized to atmosphere. This was due to non-passivity directly affects the volatilization and evaporation rates (Eq. (9)), because the dependence of the gas-liquid partition coefficients on methanol concentration (Eqs. (6) and (7)). The average volatilization flux of component $k$, $\overline{N}_0^k$, can be calculated as

$$\overline{N}_0^k = \frac{1}{S}\int_S N_0^k \, ds \qquad (16)$$

where $S$ is the area of the soil that is subject to the boundary condition of volatilization. This area is equal to $\pi(R_0^2 - r_c^2)$ (zone B) during the infiltration period (first 72 h), and $\pi R_0^2$ (zones



A and B) after infiltration (next 96 h). The accumulated mass of component $k$ released to the atmosphere from the beginning of the experiment to time $t$ can be calculated as

$$M^k(t) = S\int_0^t \overline{N}_0^k \, dt \qquad (17)$$

On the other hand, the mass of component $k$ infiltrated is equal to $M^k_{\text{inf}} = \pi r_c^2 q_{l0} C^k_{l,\text{in}} t_c$, where $t_c = 72$ h is the infiltration time. The accumulated mass of methanol released to atmosphere $M^m(t)$, normalized by the corresponding infiltrated mass of methanol $M^m_{\text{inf}}$, is shown in Fig. 8 for the three numerical experiments ($C^m_{l,\text{in}} = 5\%$, 50% and 90% w/w). This figure shows that there is no defined trend in this ratio as a function of the infiltrating mixture composition, but the curve for the more dilute mixture lies between the curves for the intermediate and the more concentrated mixtures. Even the normalized mass of methanol released to the atmosphere obtained with the 90% w/w mixture is lower than in the other $C^m_{l,\text{in}}$ cases during almost the whole period of pure volatilization (after 72 h). This apparent contradictory result can be explained by the influence of Kelvin's equation on the local volatilization flux of methanol, and consequently, on its average volatilization flux (Eq. (16)). It has been demonstrated that the Kelvin's equation (Eq. (6)) plays an important role in the solute transport near the soil surface, especially under very low water content conditions (Silva and Grifoll, 2007). Note that the local volatilization flux, $N_0{}^m$, decreases as the methanol concentration and liquid content at surface decrease. For 1D non-passive transport, Silva and Grifoll (2007) showed that the local volatilization rate suffers a sudden decrease due to the development of high capillary pressures near the surface, which reduce the gas-liquid partition coefficient according to the exponential term in Eq. (6) (Kelvin effect). At high infiltration methanol concentrations, volatilization rates are higher. This leads sooner to high capillary pressures and, therefore, to the decrease in the local volatilization flux. In the present 2D situation, a similar behavior has been observed. First, for $t < t_c$, methanol volatilizes in zone B close to $r = r_c$. During this period, in which zone A is under infiltration, the infiltrated liquid easily transports radially to zone B, close to the surface, where high liquid content (absence of Kelvin effect) and high methanol concentration lead to the high volatilization rates, as shown in Fig. 8 for $t < t_c$. One can expect that the relative methanol volatilization rate increases as the methanol concentration in the infiltrating mixture increases, as shown in Fig.

UNIVERSITAT ROVIRA I VIRGILI
TRANSPORTE NO PASIVO DE COMPUESTOS ORGÁNICOS VOLÁTILES EN LA ZONA NO SATURADA.
Orlando Silva Rojas
ISBN: 978-84-690-7612-5 / DL: T.1217-2007

8 for $C^m_{l,in}$ = 5 and 50% w/w. However, this trend is broken for $C^m_{l,in}$ = 90% w/w, which shows relative volatilization rates close to the case for $C^m_{l,in}$ = 5% w/w when $t < t_c$. This reduction in volatilization rate is due to the high viscosity for such high concentration mixture, which reduces the liquid ability to spread radially and reach the surface of zone B to undergo volatilization. Once the infiltration period has ceased ($t > t_c$), there is a short period of time (approximately from $t$ = 72 to $t$ = 76 h) in which the volatilization rates increase in all experiments due to the availability of zone A to evaporation, which was previously under infiltration. After this short period, the volatilization rate decreases gradually, since methanol must reach the surface from a progressively increased depth. The lowest relative volatilization rate corresponds again to the experiment with $C^m_{l,in}$ = 90% w/w, because the high viscosity of the mixture reduces the liquid mobility. At the end of the simulation, the percentages of the infiltrated mass of methanol that is released to the atmosphere are about 56%, 60% and 51% for $C^m_{l,\text{in}}$ = 5% w/w, 50% w/w and 90% w/w, respectively.

### *3.2. Test case 2 Heterogeneous soil*

In the second case study, three additional simulations were run in order to investigate the non-passive transport behavior of aqueous methanol mixtures into an heterogeneous soil. The same aqueous mixtures of methanol (5%, 50% and 90% w/w) were tested in this case study, and the simulations were repeated considering the same infiltration/volatilization event described in the homogeneous case. Following a similar configuration studied in previous experimental and theoretical works (Walker et al., 1998; Hofstee et al., 1998; Taylor et al., 2001; Rathfelder et al., 2001; Oostrom et al., 2003; Taylor et al., 2004; Braun et al., 2005), we consider here the soil as composed by a clay lens embedded in a main matrix of sandy clay loam texture. The clay lens was a cylinder of 0.25 m of radius and 0.1 m thick. This block is located at the center of the domain, 0.1 m below the soil surface as shown in Fig. 2b. In order to account for this particular heterogeneous configuration, the soil-water retention function and the hydraulic conductivity were constructed as 2D domain piecewise function, i.e., they are evaluated using the hydraulic properties (BC and RN parameters), specific for each soil texture.

In order to make comparisons over the same basis, it is convenient to assume that the initial mass of water in the soil is the same both in the homogeneous and heterogeneous soil



cases. Therefore, in the heterogeneous soil case, rather than a initial distribution of matric pressure, we have actually assumed as initial condition a uniform volumetric liquid content throughout the soil, by imposing different matric pressures in the main sandy clay loam matrix (-100 m) and in the clay lens (-1490 m). It is noteworthy that in the heterogeneous soil simulations, matric pressure continuity was specified at the faces of adjacent cells of different texture. This condition allowed to ensure the continuity in the liquid-phase flux at these boundaries.

Fig. 9 shows the volumetric liquid content (Fig. 9a-c) and normalized concentration (Fig. 9d-f) profiles at the end of the experiment ($t$ = 168 h) for the three infiltrating mixtures tested. As in Test case 1, the methanol concentration has been normalized with respect $C^m_{l,\text{in}}$ in order to emphasize the non-passive transport behavior (Silva and Grifoll, 2007). The first observation that can be deduced from this figure is that the non-passive transport of aqueous mixtures of methanol in a heterogeneous soil leads to significantly higher differences in both the liquid content and normalized concentration profiles, compared to the results obtained in the homogeneous soil case. This in principle was an expected result, because the soil geometry assumed in this test case enables a higher variability of the liquid-phase velocity, which at the same time is influenced by and is responsible of the non-passivity.

It is well known that small-scale structures, such as small-scale sand lenses, can influence multi-phase flow and transport significantly (Walker et al., 1998; Hofstee et al., 1998; Taylor et al., 2001; Rathfelder et al., 2001; Oostrom et al., 2003; Taylor et al., 2004; Braun et al., 2005). Many laboratory experiments have shown that capillary forces have a large impact on the two-phase flow behavior in porous media on almost all scales (Illangasekare et al., 1995; Eichel et al., 2005). These studies have shown that NAPL cannot penetrate a region of finer material as long as the capillary pressure has not yet exceeded the entry pressure (Braun et al., 2005; Eichel et al., 2005). On the contrary, we found that a water miscible solute like methanol entered into the clay lens as shown in Fig. 9d-f. Note that, however, to some degree the liquid content and concentration profiles of Fig. 9 represent a “residual saturation” of liquid and methanol at the end of the simulation, resulting after infiltration, redistribution and volatilization processes. Although only results at 168 h are shown here, we found that during infiltration the liquid mixture floods the top of the clay lens to some extent and flows above it. This was because during infiltration the lower intrinsic permeability of the lens resulted in smaller flow velocity than in the background material. Hence, the main direction of the flow changed from the vertical to the horizontal direction, if

UNIVERSITAT ROVIRA I VIRGILI
TRANSPORTE NO PASIVO DE COMPUESTOS ORGÁNICOS VOLÁTILES EN LA ZONA NO SATURADA.
Orlando Silva Rojas
ISBN: 978-84-690-7612-5 / DL: T.1217-2007

we compare this situation with the homogeneous soil case studied in section 3.1. Therefore, in many aspects, during infiltration the non-passive transport behavior of methanol-water mixtures caused by the presence of a lower permeability lens is similar to the characteristics observed in the transport of NAPL in heterogeneous soils (Braun et al., 2005).

Flow and redistribution of the liquid mixture

The same analysis of section 3.1 can be used to describe the non-passive transport behavior of aqueous mixtures of methanol in the heterogeneous soil case. Similar conclusions can be made about the consequences of non-passivity at small-scales, i.e., the differences in both volumetric liquid content and normalized concentration profiles separately developed within the clay lens and in the sandy clay loam background matrix.

The methanol volatilization was higher in the non-passive transport through the unsaturated heterogeneous soil. As in the homogeneous soil case, the infiltration of the more concentrated mixture resulted in higher concentrations of methanol within the soil, yielding a more viscous liquid mixture. The more concentrated infiltrating mixture moved more slowly and consequently, because it remained close to the surface for a longer period during infiltration ($t < 72$ h), underwent a higher volatilization. For the three infiltrating mixtures volatilization was higher than in the homogeneous soil case, because during infiltration the clay lens acted as a capillary barrier that kept the methanol closer to the surface. An increase in the lateral flow was promoted by the clay lens, which enhanced the processes of evaporation and volatilization developed along the zone B during the infiltration period. Consequently, the difference between the volatilized volume of liquid and the respective volume of water evaporated in absence of infiltration, expressed as percentage of the infiltrated volume of liquid, increased to about 50.8%, 40.3% and 39.9% for 5%, 50% and 90% w/w mixtures, respectively. Fig. 9a-c shows the drying process of the top soil was more severe in the infiltration of 90% w/w mixture. Although the volume of liquid released to atmosphere was higher for this heterogeneous configuration than in the homogeneous soil, comparison of Fig. 4a-c and Fig. 9a-c shows that the volume of liquid within the clay lens at the end of the simulation was also higher. This obviously was due to, after the infiltration period, the clay lens acts as a capillary barrier that retained the liquid within it.

For the heterogeneous soil system, the impact of concentration-dependent viscosity on liquid flow had similar consequences to those found in the homogeneous soil simulation. Fig. 9a-c clearly shows that the more dilute mixture (5% w/w) flowed faster through both the clay



lens and background material. Because its lower viscosity the lateral flow was larger. As shown in Fig. 9a, this permitted the liquid front (defined by a moisture content contour of initial liquid content) to advance also vertically around the clay lens, and even to surpass the depth of its bottom boundary ($z = 0.2$ m) within the background matrix. In the same way, within the clay lens the liquid flowed vertically and laterally much more than the 50% w/w and 90% w/w mixtures. Because the higher liquid-phase velocities, at $t = 168$ h the 5% w/w mixture reached the lateral boundary of the lens. Here, as will be discussed later, the liquid flowed downward. The liquid accumulation within the clay lens (or "residual liquid saturation") and local volumetric liquid contents were higher than in the other infiltrating mixtures. On the contrary, for the 90% w/w mixture, at $t = 168$ h there still were dry zones within the clay lens (Fig. 9c). Note that, for this mixture, the liquid content just above the clay lens was slightly higher than the moisture content in the same zone for less concentrated infiltrating mixtures, although the drying of the top soil was higher as well. This result is similar to the higher local liquid contents obtained with the 90% w/w mixture in the homogeneous case. Hence, differences in volumetric liquid content profiles resulted mainly from the concentration-dependent viscosity flow. These differences are magnified by the presence of the clay lens. Note that the differences in the liquid front advance at the clay lens scale are much higher than in the homogeneous soil system. Assuming that the liquid front within the clay lens is defined by a volumetric liquid content of $\theta_l = 0.17$ $m^3/m^3$, the difference in the liquid front position within the lens, between the less and more concentrated mixtures, is about 43%. The maximum relative difference in volumetric liquid content established between 5% and 90% w/w profiles for the heterogeneous configuration was about 142% at $z = 1.25$ cm, $r = 25.7$ cm.

Distribution of concentration and transport mechanisms

The differences in normalized concentration profiles shown in Fig. 9d-f were much higher than in the homogeneous soil case. The maximum relative difference in the normalized methanol concentration between 5% and 90% w/w profiles was about 275% at $z = 19.25$ cm, $r = 29.8$ cm. At the end of simulation, the methanol transfer limitations from inside the soil to the surface were even larger than in the homogeneous soil case for the more dilute mixtures, because the larger reduction in methanol concentration above the clay lens (first 10 cm adjacent to the soil surface). At the end of simulation ($t = 168$ h) the more reduced methanol concentrations above the clay lens caused a slight decrease in the concentration gradients

UNIVERSITAT ROVIRA I VIRGILI
TRANSPORTE NO PASIVO DE COMPUESTOS ORGÁNICOS VOLÁTILES EN LA ZONA NO SATURADA.
Orlando Silva Rojas
ISBN: 978-84-690-7612-5 / DL: T.1217-2007

compared to the homogeneous soil situation, and the more severe drying of the top soil causes a decrease in the relative permeability and so in the liquid-phase flux within this zone. Hence, the main transport mechanisms of methanol -globally dominant dispersion in the liquid-phase and locally dominant gas-phase diffusion near the top soil- decreased respect the homogeneous soil case. Figure 9d-f shows that there were significant differences in the way that methanol distributes through both the main sandy clay loam matrix and the clay lens. As previously explained, the differences in the normalized concentration of methanol above the clay lens were due to the higher lateral flow in this zone that enhances the processes of evaporation and volatilization, for the more concentrated infiltrating mixture. The differences in normalized concentration of methanol within the clay lens were caused because (a) the composition of the infiltrating mixture: infiltration of a more concentrated mixture leads to higher concentration in both the background material and the clay lens, and (b) differences in the liquid-phase velocity caused by the effect of viscosity on the unsaturated hydraulic conductivity: infiltration of a more concentrated solution yields a more viscous mixture within the clay lens, which leads to a lower radial and vertical flow in this region. Consequently, Fig. 9d shows an accumulation of methanol at the bottom of the lens provoked by larger velocities in the case of the more dilute mixture, whereas the methanol distributed within the lens in the case of the more concentrated mixture (Fig. 9f) resulted from an infiltration of a larger amount of methanol that causes a more viscous flow. As in the homogeneous soil case, the infiltration of the 90% w/w mixture for the heterogeneous configuration led to the formation of a bump of methanol concentration (Fig. 9f) and a notch in the volumetric liquid content (Fig. 9c). These irregularities were developed around and above the upper right corner of the clay lens. From Fig. 9c and 9f it is apparent that the advance of the solute front caused a notch more irregular than that obtained in the homogeneous soil case. To a large extent, this was due to the impact of composition on surface tension (Eq. (15)), which caused high capillary pressure gradients around a region of high variability in the hydraulic properties and, consequently, led to a locally large liquid flow. Hence, the effects of concentration-dependent changes in surface tension on the liquid retention curve, in transition zones of the soil between high and low concentrations, are magnified by the soil heterogeneity.

Liquid-phase velocity field

The liquid-phase velocity fields calculated at the end of the heterogeneous soil simulations are shown in Fig. 10 for the 3 infiltrating mixtures considered in the present



study. We note that the fields above the clay lens of this figure are similar to the velocity fields in the zone of upward flow that were obtained in the homogeneous soil case (Fig. 7). As in that case, the liquid flow was globally higher for the more dilute mixture (5% w/w). That is, the viscosity has globally the major impact on the liquid movement through its effect on the unsaturated hydraulic conductivity (see Eq. (2)). Additionally, the more concentrated infiltrating mixture yields a smaller liquid-phase velocity near the soil surface. Because for the heterogeneous configuration the drying of the soil was even more severe in this zone when the infiltrated mixture was more concentrated in methanol, the relative hydraulic conductivity was lower and thus, the liquid-phase flow was lower.

On the other hand, Fig. 10 shows that the more dilute mixture (5% w/w) flowed faster than the other two mixtures within the clay lens. The flow here is mainly downward and lateral. It is noteworthy that for the more dilute mixture, within the lens the direction of descending concentration gradient was precisely upward, whereas the liquid content gradient (and the matric pressure gradient) decreased downward. Due to the higher liquid-phase velocities, at $t$ = 168 h the 5% w/w mixture reached the lateral boundary of the lens, were the liquid flowed mainly downward because the capillary gradient in the radial direction at this boundary was small. The higher velocities led to a higher accumulation of liquid within the clay lens and higher local volumetric liquid contents, than those obtained with the infiltration of the other two mixtures (see Fig. 9a-c). The gradient of matric pressure in the axial direction near the upper boundary of the clay lens, was low for the intermediate mixture (50% w/w). Thus, the axial flow decreased in the in this zone of the lens, and the liquid flowed mainly in the lateral direction. In the case of the 90% w/w mixture (Fig. 10c), near the upper boundary of and within the lens, the concentration and volumetric liquid content gradients descend upward, provoking an ascending liquid flow in this zone. Also in the case of the more concentrated mixture there was a locally higher descending liquid flow around the upper right corner of the lens (Fig. 10c). As shown in Fig. 9c and 9f, there were high concentrations of methanol above the lens and low volumetric liquid content within the lens ($0.15 \leq z \leq 0.125$, $0.15 \leq r \leq 0.25$). The directions of descending concentration and moisture content gradients coincides in this region, which causes a local increase in the velocity of the liquid phase around $0.075 \leq z \leq 0.1$, $0.15 \leq r \leq 0.25$. This result is consistent with the effect of composition on soil-water retention curve (Eqs. (12) and (15)), from which it is deduced that the tendency will be for flow to occur from concentrated regions toward clean regions (Smith and Gillham, 1994, 1999; Henry and Smith, 2002). On the other hand, Fig. 10c shows that a downward

UNIVERSITAT ROVIRA I VIRGILI
TRANSPORTE NO PASIVO DE COMPUESTOS ORGÁNICOS VOLÁTILES EN LA ZONA NO SATURADA.
Orlando Silva Rojas
ISBN: 978-84-690-7612-5 / DL: T.1217-2007

flow of liquid is established below the center of the lower boundary of the lens ($z = 0.2$ m, $r \leq 0.1$ m), for the more concentrated mixture. This flow is less noticeable for $C^m_{l,\text{in}} = 50\%$ w/w (Fig. 10b) and practically negligible for $C^m_{l,\text{in}} = 5\%$ w/w (Fig. 10a). This locally higher flow coincides with an increase in the volumetric liquid content developed within this zone (Fig. 9b-c) and also is proportional to the concentration of methanol just above the lower boundary of the lens (Fig. 9e-f). To some degree, these results are similar to the behavior observed by Henry and Smith (2002), who found an increase in pressure with decreasing moisture content relationship, contrary to the common behavior of constant surface tension systems in which increases in pressure are associated with wetting events. Therefore, the transport of concentrated aqueous mixtures of methanol through an heterogeneous soil may result in an important surfactant-induced flow.

Methanol volatilization

In addition to an increase in the volatilization of the mixture due to the presence of the clay lens, there were no significant changes in the behavior of the fraction of infiltrated mass of methanol that is released to atmosphere, compared to the homogeneous soil situation. Fig. 11 shows the evolution of the ratio $M^m(t)/M^m_{\text{inf}}$, for the heterogeneous configuration. At the end of the simulation, the percentages of infiltrated mass of methanol that is released to the atmosphere were about 65%, 71% and 59% for $C^m_{l,\text{in}} = 5\%$ w/w, 50% w/w and 90% w/w, respectively. That is, in all cases, the soil heterogeneity caused an increase of about 9% in the volatilized mass of methanol, compared to the released mass obtained in the homogeneous soil case. Regardless this increase, the mechanisms responsible for the behavior of the methanol release rates are still the same that are described in section 3.1, for the homogeneous soil case. That is, the impact of Kelvin's equation (6) on the local and average volatilization fluxes of methanol (Eqs. (9) and (16)), caused by the drying of the soil surface, and the viscous effect in the case of the more concentrated mixture that reduces the mobility of the liquid to reach the surface in the zones where it volatilizes (zone B during infiltration, zones A and B after infiltration). As in the homogeneous soil case, for $t > t_c$, there is a short period of time in which the volatilization rates increase in all experiments due to the availability of zone A to volatilization/evaporation. The faster drying process and the higher viscosity caused a larger impact on the volatilization of the more concentrated infiltrating mixture than in the homogeneous soil case. As shown in Fig. 11, the normalized mass of methanol released



to the atmosphere obtained with the 90% w/w mixture was lower than in the other $C^m_{l,\text{in}}$ cases during the whole simulation.

We see that, in both homogeneous and heterogeneous soil systems, the extension and intensity of the velocity field clearly follow the distributions of liquid and methanol within the soil. In the same way, the liquid content and methanol concentration profiles reflect the dynamic of the liquid motion. Hence, the coupled non-passive transport of liquid and a solute through the unsaturated zone is a highly interactive phenomenon in which matric pressure gradients can induce solute transport and, reciprocally, mixture composition may change the transport properties and induce a given pattern of flow.

*3.3. Sensitivity to dispersion analysis*

Because the non-passive transport of alcohol-water mixtures in the vadose zone involves concentration-dependent properties, dispersivity has a direct effect on simulations (Smith and Gillham, 1994, 1999; Henry et al., 2001, 2002; Silva and Grifoll, 2007). Results obtained in the previous section, specially in the homogeneous case and more dilute mixtures, appear to be inconsistent with experimental and modeling observations of Smith and Gillham (1999), Henry and Smith (2002) and Henry et al. (2002). Unlike our simulations that predict a main flow mechanism driven by the capillary component due to variations in liquid content and due to the effect of composition on the viscosity of the liquid mixture, these authors have observed a significant impact of the concentration-dependent surface tension on unsaturated flow. This discrepancy in principle may be due to the use of a relatively large dispersivity value ($\alpha^0_{Li} = 7.8$ cm) that has caused the solute front to be highly dispersed and has substantially reduced the impact of the solute concentrations on unsaturated flow, specially in the case of low-concentration infiltrating mixtures. Nevertheless, it should be noted that the increase in the matric pressure due to the reduction of the surface tension in accordance with the scaling proposed by Leverett (1941) (Eq. (15)) is more pronounced in case of butanol aqueous solutions than with aqueous mixtures of methanol. As explained by Smith and Gillham (1994) "butanol, 0-7% by weight at 25 ºC, causes a nonlinear and relatively large change in surface tension with concentration. Methanol, 0-7% by weight at 25 ºC, causes a near linear and relatively small change in surface tension". A simple calculus shows that in the case of butanol the reduction is about 70% in the range of 0-7% by weight. Here it is

UNIVERSITAT ROVIRA I VIRGILI
TRANSPORTE NO PASIVO DE COMPUESTOS ORGÁNICOS VOLÁTILES EN LA ZONA NO SATURADA.
Orlando Silva Rojas
ISBN: 978-84-690-7612-5 / DL: T.1217-2007

noteworthy that experiments and simulations carried out by Smith and Gillham (1994, 1999), Henry and Smith (2002), Henry et al. (2002) and Henry and Smith (2006) involved scenarios of pure infiltration, unlike our simulations, which include infiltration and volatilization of the mixture. For aqueous mixtures of methanol and in the full range of solubility the reduction in surface tension is also 70%. However, for $C^m_{l,\mathrm{in}} = 90\%$ w/w, at the end of the simulations presented in the previous cases, the concentration of methanol within the soil decreased to less than 50% of this inlet composition, which involves a surface tension reduction of 52%. Then, in order to demonstrate the sensitivity of the results to dispersion, we repeated the simulation with a longitudinal dispersivity value of 1.0 cm, for both homogeneous and heterogeneous cases and the mixture of composition 90% w/w, for which more noticeable non-passive effects are expected.

Henry et al. (2002) found that their results were dependent on the longitudinal dispersivity used in the simulations. Although they only showed simulations results obtained with a longitudinal dispersivity of 1.0 cm, they clearly stated that at higher dispersivities, concentration gradients within the solute front were less sharp and resulted in smaller capillary pressure gradients near the front. On the contrary, longitudinal dispersivity values less than 1.0 cm caused sharper surfactant-induced capillary pressure gradients. In the present simulations the effect of an increase in the capillary pressure gradients due to a decrease in the longitudinal dispersivity was more pronounced than that obtained by Henry et al. (2002), because the drying of the surface in the zone B during infiltration, and also because the presence of the clay lens in the heterogeneous soil case. Unlike Henry et al. (2002) and Henry and Smith (2006), who assumed the surface as a non-flow boundary except at the point or line source of injection, our simulations considered different regions of the surface that are simultaneously under infiltration (zone A, $t \le t_c$) or volatilization (zone B). At the beginning of the infiltration period, the matric pressure gradient in the radial direction at the infiltration radius $r_c$ and near the surface was very sharp, because very wet cells were directly in contact with very dry ones. During infiltration, the matric pressure gradient in the vertical direction and near the surface is also very sharp in zone B, especially in the cells closer to the lateral boundary ($r = R_0$). This also occurs throughout the surface (zones A and B), after infiltration has ceased ($t \ge t_c$). Because these sharper capillary pressure gradients obtained with a dispersivity of 1.0 cm, during some stages of the heterogeneous soil simulation, the necessary time steps to reach the given tolerance were significantly lower than with a longitudinal dispersivity at saturation of 7.8 cm.



Homogeneous soil

Fig. 12 shows the volumetric liquid content and normalized concentration profiles, and the liquid-phase velocity field obtained at the end of the simulation with $\alpha^o_{Li} = 1.0$ cm and $C^m_{l,\mathrm{in}} = 90\%$ w/w in the homogeneous soil experiment. Both the axial and radial components of the velocity field (Fig. 12c) in the downward flow zone ($z \ge 0.15$ m) obtained with $\alpha^o_{Li} = 1.0$ cm were higher than the respective velocity components simulated with a longitudinal dispersivity of 7.8 cm (see Fig 7c). This increase in the liquid flow was caused by an increase in the capillary pressure gradient, as a consequence of the dependence of surface tension on concentration (Smith and Gillham, 1994, 1999; Henry et al., 2002). As shown in Fig 12b, for a longitudinal dispersivity of 1.0 cm the solute front is more retarded in relation to the liquid front (Fig. 12a), than in the 7.8 cm case. The zone delimited by the liquid front encompasses a very concentrated region above a very diluted one. Because for a lower dispersivity the concentration profile was not so dispersed, the concentration gradient at the solute front was higher. This concentration gradient caused an increase in the liquid fluxes, as can be deduced from Eqs. (2) and (15). As shown in Fig. 12b, very high concentrations of methanol are still encountered at $t = 168$ h. Note that the viscosity of the liquid mixture is a concave function of the concentration reaching a maximum at about $C^m_l = 392$ kg/m$^3$ (Silva and Grifoll, 2007). Simulation with $\alpha^o_{Li} = 7.8$ cm led to concentrations close to this maximum of viscosity (see Fig. 5c). Because the simulation with $\alpha^o_{Li} = 1.0$ cm resulted in higher concentrations within the soil, the viscosity of the liquid mixture was lower. Therefore, the less viscous flow added positively to the impact of surface tension on liquid flow, which caused a larger displacement of the liquid and led to lower local volumetric liquid contents than when $\alpha^o_{Li} = 7.8$ cm (see Figs. 4c and 12a).

The liquid front advanced about 4% more than in the simulation with a longitudinal dispersivity of 7.8 cm, and the volume of liquid within the soil increased in 0.6%. The less dispersed concentration gradient and the high concentrations obtained with a lower dispersivity also caused the formation of a large notch in the $z$-direction around the right upper part of the liquid content profile (Fig. 12a), which was not so obvious in the homogeneous soil with a dispersivity of 7.8 cm and the 90% w/w mixture (Fig. 4c). At the same time, an opposite behavior in the velocity field occurred near the surface below zone A, in the upward flow zone ($z < 0.15$ m). That is, the liquid-phase velocities simulated with a

UNIVERSITAT ROVIRA I VIRGILI
TRANSPORTE NO PASIVO DE COMPUESTOS ORGÁNICOS VOLÁTILES EN LA ZONA NO SATURADA.
Orlando Silva Rojas
ISBN: 978-84-690-7612-5 / DL: T.1217-2007

dispersivity value of 1.0 cm were lower than those obtained with a higher dispersivity. This was due to a combination of two effects: viscosity-dependent flow and reduction of the relative permeability. As much higher concentrations of methanol were available close to the surface for a lower dispersivity, the liquid flow was even more viscous and slower than the respective flow when $\alpha_{Li}^{o}$ = 7.8 cm in this region. Likewise, these higher concentrations cause the top soil to dry faster. Hence, the unsaturated hydraulic conductivity is reduced and, consequently, the liquid-phase velocity is lower. Note that, however, the liquid flow was higher than that resulted with a higher dispersivity, near the soil surface in zone B, just coinciding with the solute front advance. Again, this increase was due to the reduction in surface tension under relatively high concentrations that induced a higher liquid flow upward for $\alpha_{Li}^{o}$ = 1.0 cm. This locally high liquid flow made the liquid front go up around $r$ = 0.25 m, in this zone (Fig. 12a).

On the other hand, because higher concentrations of methanol were available near the surface during the simulation when $\alpha_{Li}^{o}$ = 1.0 cm, volatilization of methanol was higher. Thus, the difference between the volatilized liquid and the water evaporated in absence of infiltration, expressed as percentage of the infiltrated volume of liquid increased to 42.9%. Note that the more severe drying promoted by high concentrations of methanol close to the surface induced a larger reduction on the local volatilization fluxes, according to Kelvin's equation (6). Hence, the rate of accumulated volatilization of methanol experimented a significant decreasing. Despite this reduction, the percentage of the infiltrated mass of methanol that volatilizes to the atmosphere, at the end of the simulation, increased from 51%, for $\alpha_{Li}^{o}$ = 7.8 cm, to 54%, for $\alpha_{Li}^{o}$ = 1.0 cm.

It is noteworthy that with a lower dispersivity, convection in the liquid-phase was the global predominant mechanism that drove the methanol transport. Also, due the larger drying of the soil surface, gas-phase diffusion of methanol was more active near the surface than with a dispersivity of 7.8 cm. These results are similar to those found by Silva and Grifoll (2007), who simulated the 1D non-passive transport of aqueous mixtures of methanol in a sandy clay loam soil. Their 1D simulations with a dispersivity of 0.2 cm showed that convection was more active for methanol transport than dispersion, and the capillary liquid flux due to changes in the composition was the predominant mechanism of liquid flow in the solute-front region.



Heterogeneous soil

The effect of a lower dispersivity on the non-passive transport of a concentrated aqueous mixture of methanol ($C_{l,\text{in}}^{m}$ = 90% w/w) in the heterogeneous soil is shown in Fig. 13. Comparing the volumetric liquid content profiles of Figs. 9c and 13a, we observe that for $\alpha_{Li}^{o}$ = 1.0 cm the liquid flowed easier through both the sandy clay loam matrix and the clay lens, than when the dispersivity was set to $\alpha_{Li}^{o}$ = 7.8 cm. On the one hand, Fig. 13a shows first that, the liquid front arrived to the right boundary of the lens through the main soil matrix. Secondly, as in the homogeneous soil simulation with a lower dispersivity, the liquid front went up near the soil surface along the zone B ($r$ = 0.25 m). On the other hand, within the lens the liquid front advanced such that the very dry zone around the upper right corner of the lens, found with a higher dispersivity, disappeared in the $\alpha_{Li}^{o}$ = 1.0 cm-simulation.

Locally lower volumetric liquid contents were found for the lower dispersivity both above and below the upper boundary of the lens, although the total volume of liquid within the soil increased in 0.8%. To some extent, the volumetric liquid content profile simulated with $\alpha_{Li}^{o}$ = 1.0 cm and $C_{l,\text{in}}^{m}$ = 90% w/w is similar to the liquid content profile obtained with $\alpha_{Li}^{o}$ = 7.8 cm and $C_{l,\text{in}}^{m}$ = 50% w/w. As in the homogeneous soil case, these results are due to the combined effect of viscosity and surface tension concentration-dependent flow, which affect the liquid-phase fluxes according to the distribution of methanol within the soil (Fig. 13b). Note that the very high concentrated zone above the clay lens creates a less viscous flow that helps to increase even more the surface tension-induced upward flow caused by the high concentration gradients in this region. On the contrary, methanol concentrations within the clay lens were higher than when $\alpha_{Li}^{o}$ = 7.8 cm, and they were in the range of increasing viscosity as well. However, the more viscous flow was insufficient to counteract the surface tension-induced flow caused by the higher concentration gradients developed for $\alpha_{Li}^{o}$ = 1.0 cm. This enhance in the liquid flux can be seen comparing the velocity fields of Figs. 10c and 13c, mainly as a broader zone of flow within the clay lens and an increase in the upward flow of liquid near the surface in zone B ($r$ = 0.25 m), when $\alpha_{Li}^{o}$ = 1.0 cm. Analogous to the homogeneous soil situation, for this value of dispersivity the volatilization of methanol was higher than when $\alpha_{Li}^{o}$ = 7.8 cm. Therefore, the percentage of the infiltrated liquid corresponding to the difference between the volatilized liquid and the water evaporated in absence of infiltration increased to 50.5%, while the percentage of the infiltrated mass of

UNIVERSITAT ROVIRA I VIRGILI
TRANSPORTE NO PASIVO DE COMPUESTOS ORGÁNICOS VOLÁTILES EN LA ZONA NO SATURADA.
Orlando Silva Rojas
ISBN: 978-84-690-7612-5 / DL: T.1217-2007

methanol that volatilizes to the atmosphere, at the $t = 168$ h, increased from 54%, for $\alpha_{Li}^{o} = 7.8$ cm, to 64%, for $\alpha_{Li}^{o} = 1.0$ cm.

Nevertheless, unlike the homogeneous soil experiment with a lower dispersivity, at the end of the heterogeneous soil simulation with $\alpha_{Li}^{o} = 1.0$ cm, dispersion in the liquid-phase was again globally the predominant methanol transport mechanism. This was due to the clay lens and the more severe drying of the top soil caused an increase in the concentration gradients above the lens. Diffusion of methanol in the gas-phase was again more active in the top soil than with the dispersivity was set to 7.8 cm, because the higher drying of the surface promoted by the clay lens and higher methanol concentrations.

## 4. Conclusions

The unsaturated flow and non-passive transport model for water-soluble organic compounds previously developed by Silva and Grifoll (2007), was implemented in cylindrical coordinates with a top boundary condition that accounts for different zones of the soil surface to simultaneously be under infiltration or volatilization. The model has been used to illustrate the infiltration, redistribution and volatilization/evaporation of methanol-water mixtures both into 2D homogeneous and heterogeneous unsaturated soils. Simulation scenarios of this study involved the infiltration of three aqueous solutions of methanol with compositions 5%, 50% and 90% w/w, into a homogeneous sandy clay loam soil and a heterogeneous soil consisted of a clay lens embedded within a background material of sandy clay loam texture. Our 2D results confirm those of Silva and Grifoll (2007) found for 1D non-passive systems. Simulations of the test cases showed that the extension and intensity of the velocity field clearly respond to the distribution of the liquid and methanol within the soil. In the same way, the liquid content and methanol concentration profiles reflected the dynamic of the liquid flow. Therefore, the coupled non-passive transport of liquid and solute through the unsaturated zone should be viewed as a highly interactive phenomenon. Matric pressure gradients can induce solute transport. Reciprocally, the mixture composition may change the transport properties and induce a given pattern of flow.

The main properties influenced by the mixture composition were: (a) the viscosity and surface tension, which directly affected the liquid flow; (b) the density that led to the non-ideal mixing of the inlet mixture with the initial soil moisture; and (c) the gas-liquid partition



coefficients, which had a significant impact on the mass transfer limitations from inside the soil to the surface and, consequently, on the overall volatilization rates. Note that since the viscosity is a concave function of the methanol concentration, the liquid flux increased or decreased according to the range of concentrations developed within the soil. This caused the viscous effect to act in the same or the opposite direction of the flow induced by the surface tension, depending on the amounts of methanol and the magnitude of the concentration gradients developed in the soil. This interaction of effects occurred at each scale in the heterogeneous soil simulation.

For a dispersivity of 7.8 the predominant mechanism that globally drives the transport of methanol was dispersion in the liquid-phase, with a locally dominant gas-phase diffusion close to the soil surface. Under this circumstances, the of more dilute infiltrating mixtures flowed faster due to their lower viscosity. On the contrary, more concentrated infiltrating mixtures resulted in a more slowly movement and consequently, took much longer in reaching the zones of the soil surface where volatilization occurs (zone A, during infiltration; zones A and B, after that). Because, in addition, the lowering effect of Kelvin's equation on the gas-liquid partition coefficients directly influenced the local volatilization fluxes of methanol and evaporation of water, the fraction of infiltrated mass of methanol that is released to the atmosphere was much more affected, in the case of more concentrated infiltrating mixture. At the end of the simulation, there was a maximum difference of almost 10% in the volatilized mass of methanol between the intermediate and more concentrated mixtures. For homogeneous soil experiments, the relative large dispersivity at saturation reduced the impact of concentration on the flow induced by changes in surface tension. Nevertheless, the infiltration of the more concentrated mixture led to a notch in the liquid content profile that coincided with the formation of a bump in the methanol concentration profile. This implies that, despite the large dispersivity value used in the simulations, the infiltration of concentrated mixtures of methanol could result in important surfactant-induced liquid flow. At the end of the simulation, the maximum relative difference in volumetric liquid content between 5% and 90% w/w profiles was about 155%, whereas the maximum relative difference in the normalized concentration of methanol was about 173%.

Heterogeneity was a key factor that favored the non-passivity in the transport of aqueous mixtures of methanol. Differences in volumetric liquid content and normalized concentration of methanol became more pronounced during the non-passive transport in an heterogeneous soil. The clay lens embedded into the sandy clay loam matrix acted as a

ISBN: 978-84-690-7612-5 / DL: T.1217-2007

capillary barrier that caused the mixture be close to the surface for a longer time during infiltration, and retained high amounts of liquid within it during pure volatilization period. Also the lens promoted the development of important gradients of concentration during the infiltration and redistribution of more concentrated mixtures, which caused an increase in the matric pressure gradients due to changes in composition. Consequently, this yielded higher surfactant-induced fluxes than in the homogeneous case. The notch in the moisture profile and the bump of concentration were also more pronounced. The difference between the volatilized volume of liquid and that evaporated in absence of infiltration, expressed as percentage of the infiltrated volume of liquid, increased in the heterogeneous soil experiment. This increasing was 12.1%, 9.2% and 6% for the $C^{m}_{l,\mathrm{in}}$ = 5, 50 and 90% w/w mixtures, respectively. At the end of the simulation, the maximum relative difference in volumetric liquid content between 5% and 90% w/w profiles was about 142%, whereas the maximum relative difference in the normalized concentration of methanol was about 275%. For the three mixtures studied the volatilized mass of methanol increased in almost 10% compared to the homogeneous soil experiment. The maximum difference in the volatilized mass of methanol between the intermediate and more concentrated mixtures increased to 12%.

The sensitivity analysis of results to dispersion showed that for lower dispersivities, convection in the liquid-phase was more active than dispersion for methanol transport in the homogeneous soil experiment and the 90% w/w mixture, for which non-passivity was more noticeable. On the contrary, for the heterogeneous soil simulation dispersion in the liquid-phase was again the dominant transport mechanism, since the clay lens and a higher drying of the soil surface caused an increase in the concentration gradients above the lens. Simulations with a dispersivity value of 1.0 cm showed that changes in the capillary pressure caused by changes in the mixture composition were higher than with a dispersivity of 7.8 cm. In the homogeneous soil case, this was reflected by an increase of 8% in the advance of the liquid front, a grow of the notch in the volumetric liquid content profile, and an increase in the liquid fluxes in regions of high concentration gradients. These enhance in the liquid flow also occurred within the clay lens and through some regions of the sandy clay loam matrix, during the heterogeneous soil simulation. Additionally, for a lower dispersivity the Kelvin effect had a larger impact on the volatilization fluxes. This was because under higher concentrations of methanol near the surface the drying process was faster, which led sooner to high capillary pressure at surface and the reduction of the gas-liquid partition coefficient. Despite this sooner change in the rate of the methanol volatilization, because these higher concentrations, the



volatilized mass of methanol at the end of the simulation increased about 5% in both homogeneous and heterogeneous soil experiments with a dispersivity at saturation set to 1.0 cm.

**Acknowledgments**

We gratefully acknowledge the financial assistance received from the DGICYT of Spain, under project FIS2005-07194 and from the Generalitat de Catalunya (2005SGR-00735). We also acknowledge the support received from the DURSI and the European Social Fund.

**References**

Abbasi, F., Simunek, J., Feyen, J., van Genuchten, M.Th., Shouse, P.J.,2003. Simultaneous inverse estimation of soil hydraulic and solute transport parameters from transient field experiments: homogeneous soil. T. ASAE 46(4), 1085-1095.

Allred, B., Brown, G.O., 1996a. Anionic surfactant transport characteristics in unsaturated soil. Soil Science 161(7), 415-425.

Allred, B., Brown, G.O, 1996b. Boundary condition and soil attribute impacts on anionic surfactant mobility in unsaturated soil. Ground Water 34(6), 964-971.

Baggio, P., Bonacina, C., Schrefler, B.A., 1997. Some considerations on modeling heat and mass transfer in porous media. Transport Porous Med. 28, 233-251.

Bear, J., Bachmat, Y., 1991. Introduction to modeling of transport phenomena in porous media. Dordrecht: Kluwer.

Biggar, J.W., Nielsen, D.R., 1976. Spatial variability of the leaching characteristics of a field soil. Water Resour. Res. 1, 78-84.

Boufadel, M.C., Suidan, M.T., Venosa, A.D., 1997. Density-dependent flow in one dimensional variably-saturated media. J. Contam. Hydrol. 202, 280-301.

Boufadel, M.C., Suidan, M.T., Venosa, A.D., 1999. A numerical model for density-and-viscosity-dependent flows in two-dimensional variably saturated porous media. J. Contam. Hydrol. 37, 1-20.

UNIVERSITAT ROVIRA I VIRGILI
TRANSPORTE NO PASIVO DE COMPUESTOS ORGÁNICOS VOLÁTILES EN LA ZONA NO SATURADA.
Orlando Silva Rojas
ISBN: 978-84-690-7612-5 / DL: T.1217-2007

Braun, C., Helmig, R., Manthey, S., 2005. Macro-scale effective constitutive relationships for two-phase processes in heterogeneous porous media with emphasis on the relative permeability-saturation relationship. J. Contam. Hydrol. 76, 47-85.

Brutsaert, W., 1975. A theory for local evaporation (or heat transfer) from rough and smooth surfaces at ground level. Water Resour. Res. 11(4), 543-550.

Burdine, N.T., 1953. Relative permeability calculations from pore-size distribution data. Petroleum Trans.198, 71-77.

Burns, E.R., Parlange, J.-Y., Selker, J.S., Guenther, R.B., 2006a. Thermodynamic correction for salts in variably saturated porous media. Transport Porous Med. 63, 381-398.

Burns, E.R., Parlange, J.-Y., Selker, J.S., Guenther, R.B., 2006b. Effects of sodium chloride on constitutive relations in variable saturated porous media. Water Resour. Res. 42, W05405, doi:10.1029/2005WRRR004060.

Chen, D., Rolston, D.E., Yamaguchi, T., 2000. Calculating partition coefficients of organic vapors in unsaturated soil and clays. Soil Science 165(3), 217-225.

Chen, D., Rolston, D.E., 2000. Coupling diazinon volatilization and water evaporation in unsaturated soils: II. Diazinon transport. Soil Science 165(9), 690-698.

Da Silva, M.L.B., Alvarez, P.J.J., 2002. Effects of ethanol versus MTBE on benzene, toluene, ethylbenzene, and xylene natural attenuation in aquifer columns. J. Envir. Engrg. 128(9), 862-867.

Deeb, R.A., Sharp, J.O., Stocking, A., McDonald, S., West, K.A., Laugier, M., Alvarez, P.J.J., Kavanaugh, M.C., Alvarez-Cohen ,L., 2002. Impact of ethanol on benzene plume lengths: microbial and modeling studies. J. Envir. Engrg.128(9), 868-875.

Defay, R., Prigogine, I., Bellemans, A., Everett, D.H., 1966. Surface tension and adsorption. London: Longmans, Green & Co Ltd.

Eichel, H., Helmig R., Neuweiler, I., Cirpka, O.A., 2005. Upscaling of two-phase flow processes in porous media. In Upscaling multiphase flow in porous media, from pore to core and beyond. Ed. D.B. Das and S.M. Hassanizadeh. Dordrecht: Springer.

Ferreira, S.B., Zuquette, L.V., Grathwohl, P., 2001. Experimental investigations of oxygenated gasoline dissolution. J. Envir. Engrg. 127(3), 208-16.

Friedel, M.J., 2000. Documentation and verification of VST2D. A model for simulating transient, variably saturated, coupled water-heat-solute transport in heterogeneous, anisotropic, 2-dimensional, ground-water systems with variable fluid density. U.S. Geol. Surv. Water-Resour. Invest.Rep. 00-4105,124 pp.



Gastó, J.M., Grifoll, J., Cohen Y., 2002. Estimation of internodal permeabilities for numerical simulation of unsaturated flows. Water Resour. Res. 38(12), 1326, doi:10.1029/2002WR001529.

Gawin, D., Pesavento, F., Schrefler, B.A., 2002. Modelling of hygro-thermal behaviour and damage of concrete at temperature above the critical point of water. Int. J. Numer. Anal. Meth. Geomech. 26, 537-562.

Gmehling, J., Onken, U., Rarey-Nies, J.R., 1988. Vapor-liquid equilibrium data collection. Aqueous systems. Vol. I, part 1b (Supplement 2). Frankfurt: DECHEMA.

Grifoll, J., Cohen, Y., 1996. Contaminant migration in the unsaturated soil zone: the effect of rainfall and evapotranspiration. J. Contam. Hydrol. 23, 185-211.

Grifoll, J., Gastó, J.M., Cohen, Y., 2005. Non-isothermal soil water transport and evaporation. Adv. Water. Resour. 28(11), 1254-1266.

Henry, E.J., Smith, J.E., Warrick, A.W, 1999. Solubility effects on surfactant-induced unsaturated flow through porous media. J. Hydrol. 223, 164-174.

Henry, E.J., Smith, J.E., Warrick, A.W., 2001. Surfactant effects on unsaturated flow in porous media with hysteresis: horizontal column experiments and numerical modeling. J. Hydrol. 245, 73-88.

Henry, E.J., Smith, J.E., 2002. The effect of surface-active solutes on water flow and contaminant transport in variably saturated porous media with capillary fringe effects. J. Contam. Hydrol. 56, 247-270.

Henry, E.J., Smith, J.E., Warrick, A.W., 2002. Two-dimensional modeling of flow and transport in the vadose zone with surfactant-induced flow. Water Resour. Res. 38(11), 33-1 – 33-16.

Henry, E.J., Smith, J.E., 2006. Numerical demonstration of surfactant-concentration dependent capillarity and viscosity effects on infiltration from a constant flux line source. J. Hydrol. 329, 63-74.

Hofstee, C., Oostrom, M., Dane, J.H., Walker, R.C., 1998. Infiltration and redistribution of perchloroethylene in partially saturated, stratified porous media. J. Contam. Hydrol. 34, 293-313.

Illangasekare, T.H., Ramsay, J.L., Jensen, K.H., Butts, M.B., 1995. Experimental study of movement and distribution of dense organic contaminants in heterogeneous aquifers. J. Contam. Hydrol. 20, 1-25.

UNIVERSITAT ROVIRA I VIRGILI
TRANSPORTE NO PASIVO DE COMPUESTOS ORGÁNICOS VOLÁTILES EN LA ZONA NO SATURADA.
Orlando Silva Rojas
ISBN: 978-84-690-7612-5 / DL: T.1217-2007

Jaynes, D.B., 1991. Field study of bromacil transport under continuous-flood irrigation. Soil Sci. Soc. Am. J. 55, 658-664.

Jin, Y., Jury, A., 1996. Characterizing the dependence of gas diffusion coefficient on soil properties. Soil Sci. Soc. Am. J. 60, 66-71.

Kelley, C.T., 1995. Iterative methods for linear and nonlinear equations. Philadelphia: SIAM.

Kyle, B.G., 1999. Chemical and process thermodynamics. New Jersey: Prentice Hall.

Lenhard, R.J., Oostrom, M., Simmons, C.S., White, M.D., 1995. Investigation of density-dependent gas advection of trichloroethylene: experiment and a model validation exercise. J. Contam. Hydrol. 19, 47-67.

Leverett, M.C., 1941. Capillary behavior in porous solids, Trans. AIME 142:152-169.

Lide, D.R., 1994, Kehiaian, H.V., 1994. CRC Handbook of thermophysical and thermochemical data. CRC Press.

McDowell, C.J., Powers, S.E., 2003. Mechanisms affecting the infiltration and distribution of ethanol-blended gasoline in the vadose zone. Environ Sci. Technol. 37(9),1803-1810.

Morel-Seytoux, H.J., Nimmo, J.R., 1999. Soil water retention and maximum capillary drive from saturation to oven dryness. Water Resour. Res. 35(7), 2031-2041.

Nielsen, D.R., Biggar, J.W., 1973. Spatial variability of field-measured soil-water properties. Hilgardia 42(7), 215-259.

Oostrom, M., Hofstee, C., Lenhard, R.J., Wietsma, T.W., 2003. Flow behavior and residual saturation formation of liquid carbon tetrachloride in unsaturated heterogeneous porous media. J. Contam. Hydrol. 64, 93-112.

Ouyang, Y., Zheng, Ch., 1999. Density-driven transport of dissolved chemicals through unsaturated soil. Soil Science 164(6), 376-390.

Pan, L., Wieranga, P.J., 1997. Improving numerical modeling of two-dimensional water flow in variably saturated, heterogeneous porous media. Soil Sci. Soc. Am. J. 61(2), 335-346.

Patankar, S.V., 1980. Numerical heat transfer and fluid flow. New York: McGraw-Hill.

Press, W.H., Teukolsky, S.A., Vetterling, W.T., Flannery, B.P., 1986-1992. Numerical recipes in fortran 77: the art of scientific computing. New York: Cambridge University Press.

Ramsburg, C.A., Pennell, K.D., 2002. Density-modified for DNAPL source zone remediation: density conversion and recovery in heterogeneous aquifer cells. Environ Sci. Technol. 36(14), 3176-3187.



Ramsburg, C.A., Pennell, K.D., Kibbey, T.C.G., Hayes, K.F., 2004. Refinement of the density-modified displacement method for efficient treatment of tetrachloroethene source zones. J. Contam. Hydrol. 74, 105-131.

Rathfelder, K.M., Abriola, L.M., Taylor, T.P., Pennell, K.D., 2001. Surfactant enhanced recovery of tetrachloroethylene from a porous medium containing low permeability lenses: 2. Numerical simulation. J. Contam. Hydrol. 48, 351-374.

Rawls, W.J., Brakensiek, D.L., 1989. Estimation of soil water retention and hydraulic properties. Unsaturated flow in hydrology modeling, theory and practice. Kluwer Academic Publishers.

Reid, R.C., Prausnitz, J.M., Poling, B.E., 1987. The properties of gases and liquids. New York: McGraw-Hill Inc..

Robert, T., Martel, R., Conrad, S.H., Lefebvre, R., Gabriel, U., 2006. Visualization of TCE recovery mechanisms using surfactant-polymer solutions in a two-dimensional heterogeneous sand model. J. Contam. Hydrol. 86, 3-31.

Rossi, C., Nimmo, J.R., 1994. Modeling of soil water retention from saturation to oven dryness. Water Resour. Res. 30(3), 701-708.

Rowlinson, J.S., Widom, B., 1984. Molecular theory of capillarity. Oxford: Clarendon Press.

Schrefler, B.A., 2004. Multiphase flow in deforming porous material. Int. J. Numer. Anal. Meth. Geomech. 60, 27-50.

Schroth, M.H., Istok, J.D., Selker, J.S., Oostrom, M., White, M.D., 1998, Multifluid flow in bedded porous media: laboratory experiments and numerical simulations. Adv. Water. Resour. 22(2), 169-183.

Shapiro, A.A., Stenby, E.H., 1997. Kelvin equation for non-ideal multicomponent mixture. Fluid Phase Equilibria 134, 87-101.

Silva, O., Grifoll, J., 2007. Non-passive transport of volatile organic compounds in the unsaturated zone. Adv. Water. Resour. 30, 794-807.

Smith, J.E., Gillham, R.W., 1994. The effect of concentration-dependent surface tension on the flow of water and transport of dissolved organic compounds: A pressure head-based formulation and numerical model. Water Resour. Res. 30(2), 343-354.

Smith, J.E., Gillham, R.W., 1999. Effects of solute concentration-dependent surface tension on unsaturated flow: Laboratory sand column experiments. Water Resour. Res. 35(4), 973-982.

ISBN: 978-84-690-7612-5 / DL: T.1217-2007

Taylor, T.P., Pennell, K.D., Abriola, L.M., Dane, J.H., 2001. Surfactant enhanced recovery of tetrachloroethylene from a porous medium containing low permeability lenses: 1. Experimental studies. J. Contam. Hydrol. 48, 325-350.

Taylor, T.P., Rathfelder, K.M., Pennell, K.D., Abriola, L.M., 2004. Effects of ethanol addition on miscellar solubilization and plume migration during surfactant enhanced recovery of tetrachloroethene. J. Contam. Hydrol. 69, 73-99.

Valsaraj, K.T., 1995. Elements of environmental engineering. Thermodynamics and kinetics. Boca Raton: CRC Press Inc..

Walker, R.C., Hofstee, C., Dane, J.H., Hill, W.E., 1998. Surfactant enhanced removal of PCE in a partially saturated, stratified porous media. J. Contam. Hydrol. 34, 31-46.

Wang, Z., Feyen, J., 1998. Susceptibility and predictability of conditions for preferential flow. Water Resour. Res. 34(9), 2169-2182.

Weisbrod, N., Niemet, M.R., McGinnis, T., Selker, J.S., 2003. Water vapor transport in the vecinity of imbibing saline plumes: Homogeneous and layered unsaturated porous media. Water Resour. Res. 39(6), 1145 (doi: 10.129/2002WR001539).

Weisbrod, N., Niemet, M.R., Rockhold, M.L., McGinnis, T., Selker, J.S., 2004. Migration of saline solutions in variably saturated porous media. J. Contam. Hydrol. 72, 109-133.

White, M.D., Oostrom, M., 2000. STOMP: Subsurface transport over multiple phases. Theory guide. PNNL-12030. Pac. Northw. Natl. Lab., Richland, WA.

Wildenschild, D., Jensen, K.H., 1999a. Laboratory investigations of effective flow behavior in unsaturated heterogeneous sands. Water Resour. Res. 35(1), 17-27.

Wildenschild, D., Jensen, K.H., 1999b. Numerical modeling of observed effective flow behavior in unsaturated heterogeneous sands. Water Resour. Res. 35(1), 29-42.

Zhang, G., Zheng, Z., Wan, J., 2005. Modeling reactive geochemical transport of concentrated aqueous solutions. Water Resour. Res. 41(W02018), 1-14.

**Table 1. Simulation conditions and hydraulic soil properties**

| | | |
|---|---|---|
| Simulation conditions | | |
| Soil types | sandy clay loam (SCL), clay (C) | |
| Soil depth (m) | 0.5 | |
| Soil radius (m) | 0.5 | |
| Initial pressure head (m), $P_{M,\mathrm{ini}}$ | -100 (SCL), -1490 (C) | |
| Infiltration rate (cm/h), $q_{l0}$ | 0.3 | |
| Total time of simulation (h) | 168 | |
| Initial period of infiltration (h) | 72 | |
| Dispersivity at saturation (cm), $\alpha_{Li}^{o}$ | 7.8, 1.0 | |
| [a]Atmosphere side mass transfer coefficient for methanol (kg/m$^2$ s), $k_0^m$ | $3.5\times10^{-3}$ | |
| [a]Atmosphere side mass transfer coefficient for water (kg/m$^2$ s), $k_0^w$ | $4.0\times10^{-3}$ | |
| Hydraulic soil properties | | |
| Soil type | sandy clay loam | clay |
| [b]Soil porosity, $\varepsilon$ | 0.33 | 0.385 |
| [b]Residual water content, $\theta_{lr}$ | 0.068 | 0.09 |
| [b]Brooks-Corey parameter, $\lambda$ | 0.25 | 0.131 |
| [b]Bubble pressure, $P_{bw}$ (Pa) | 2754 | 3658 |
| [b]Hydraulic saturated conductivity, $K_s$ (cm/h) | 0.43 | 0.06 |
| [c]Volumetric liquid content at junction, $\theta_{lj}$ | 0.1415 | 0.3205 |
| [c]Rossi-Nimmo parameter, $\alpha_{RN}$ | 0.0557 | 0.0784 |

**[a]Calculated according to Brutsaert (1975) assuming a wind velocity of 2 m/s and a surface roughness length of 1 cm.**
**[b]From Rawls and Brakensiek (1989).**
**[c]Calculated according to Morel-Seytoux and Nimmo (1999).**

UNIVERSITAT ROVIRA I VIRGILI
TRANSPORTE NO PASIVO DE COMPUESTOS ORGÁNICOS VOLÁTILES EN LA ZONA NO SATURADA.
Orlando Silva Rojas
ISBN: 978-84-690-7612-5 / DL: T.1217-2007

**Figure captions**

**Figure 1.** General diagram of the cylindrical coordinate system with initial and boundary conditions assumed in this study.

**Figure 2.** Model domain with boundary an initial conditions assumed in the test cases: (a) homogeneous soil (b) heterogeneous soil.

**Figure 3.** Dependency of the concentration (a) and liquid content (b) at surface on the grid spacing $\Delta z$. Simulations with $N_r = 43$ and $\Delta t_{max} = 160$ s.

**Figure 4.** Infiltration, redistribution and volatilization of three methanol-water mixtures into an homogeneous soil. Simulation results after 168 hours and a dispersivity of 7.8 cm. Volumetric liquid content profiles for (a) 5% w/w mixture. (b) 50% w/w mixture. (c) 90% w/w mixture. Normalized concentration profiles for (d) 5% w/w mixture. (e) 50% w/w mixture. (f) 90% w/w mixture.

**Figure 5**. Liquid-phase viscosity profiles at the end of simulation of Test case 1: homogeneous soil. (a) 5% w/w mixture. (b) 50% w/w mixture. (c) 90% w/w mixture.

**Figure 6**. Volumetric liquid content profile obtained at the end of simulation for homogeneous soil and the 90% w/w mixture with constant viscosity.

**Figure 7.** Liquid-phase velocity fields for Test case 1: homogeneous soil. (a) 5% w/w mixture. (b) 50% w/w mixture. (c) 90% w/w mixture.

**Figure 8**. Evolution of normalized mass of methanol released to the atmosphere in the Test case 1: homogeneous soil.

**Figure 9.** Infiltration, redistribution and volatilization of three methanol-water mixtures into an heterogeneous soil. Simulation results after 168 hours and a dispersivity of 7.8 cm. Volumetric liquid content profiles for (a) 5% w/w mixture. (b) 50% w/w mixture. (c) 90% w/w mixture. Normalized concentration profiles for (d) 5% w/w mixture. (e) 50% w/w mixture. (f) 90% w/w mixture.



**Figure 10.** Liquid-phase velocity fields for Test case 2: heterogeneous soil. (a) 5% w/w mixture. (b) 50% w/w mixture. (c) 90% w/w mixture. The rectangle defines the boundaries of the clay lens.

**Figure 11.** Evolution of normalized mass of methanol released to the atmosphere Test case 2: heterogeneous soil.

**Figure 12.** Sensitivity to dispersion analysis. Results for the infiltration of a mixture with composition $C_{l,\mathrm{in}}^{m} = 90\%$ w/w, into an homogeneous soil with a dispersivity of 1.0 cm. Results after 168 hours of simulation. (a) Volumetric liquid content. (b) Normalized concentration of methanol. (c) Liquid-phase velocity field.

**Figure 13.** Sensitivity to dispersion analysis. Results for the infiltration of a mixture with composition $C_{l,\mathrm{in}}^{m} = 90\%$ w/w, into an heterogeneous soil with a dispersivity of 1.0 cm. Results after 168 hours of simulation. (a) Volumetric liquid content. (b) Normalized concentration of methanol. (c) Liquid-phase velocity field (the rectangle defines the boundaries of the clay lens).

UNIVERSITAT ROVIRA I VIRGILI
TRANSPORTE NO PASIVO DE COMPUESTOS ORGÁNICOS VOLÁTILES EN LA ZONA NO SATURADA.
Orlando Silva Rojas
ISBN: 978-84-690-7612-5 / DL: T.1217-2007

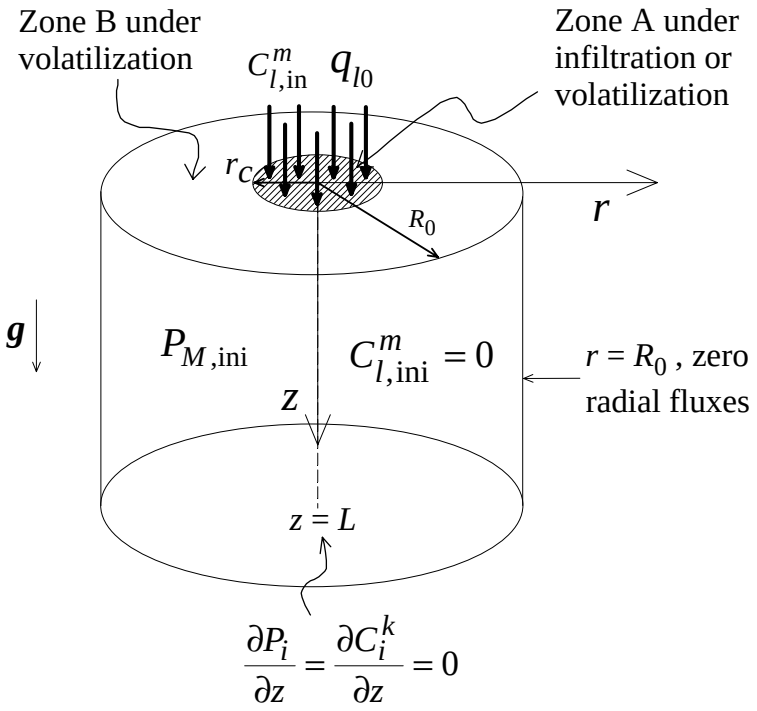


**Figure 1**





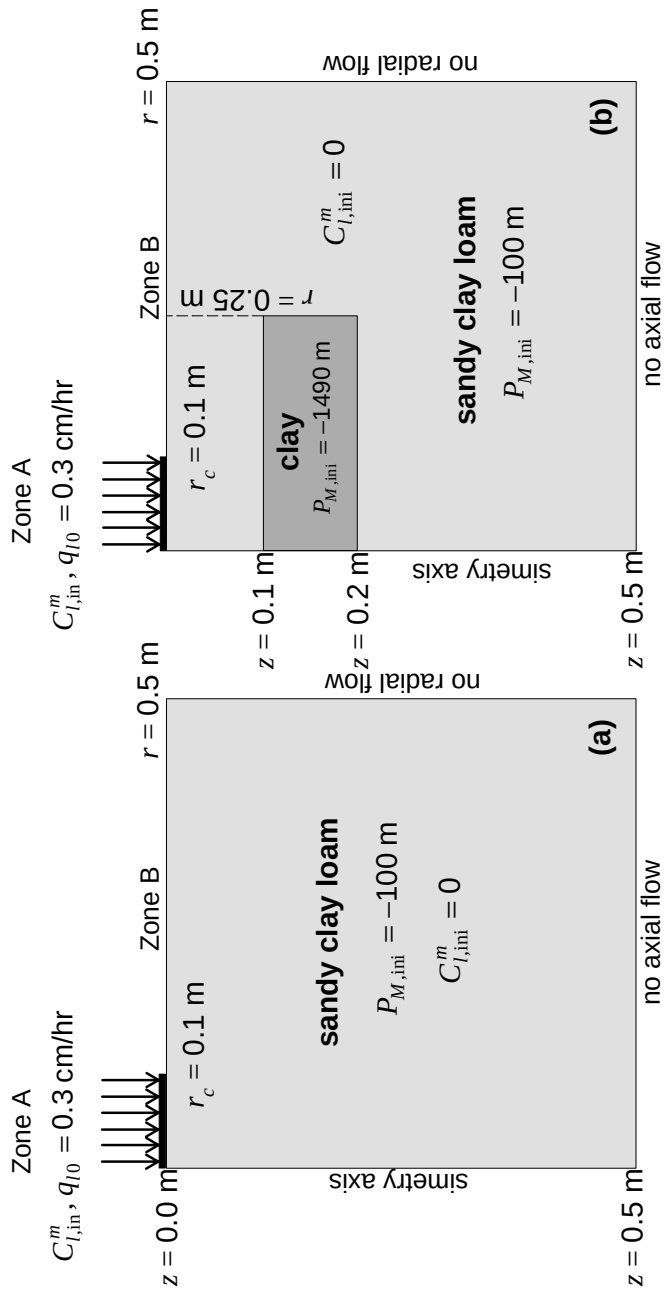


**Figure 2**

UNIVERSITAT ROVIRA I VIRGILI
TRANSPORTE NO PASIVO DE COMPUESTOS ORGÁNICOS VOLÁTILES EN LA ZONA NO SATURADA.
Orlando Silva Rojas
ISBN: 978-84-690-7612-5 / DL: T.1217-2007

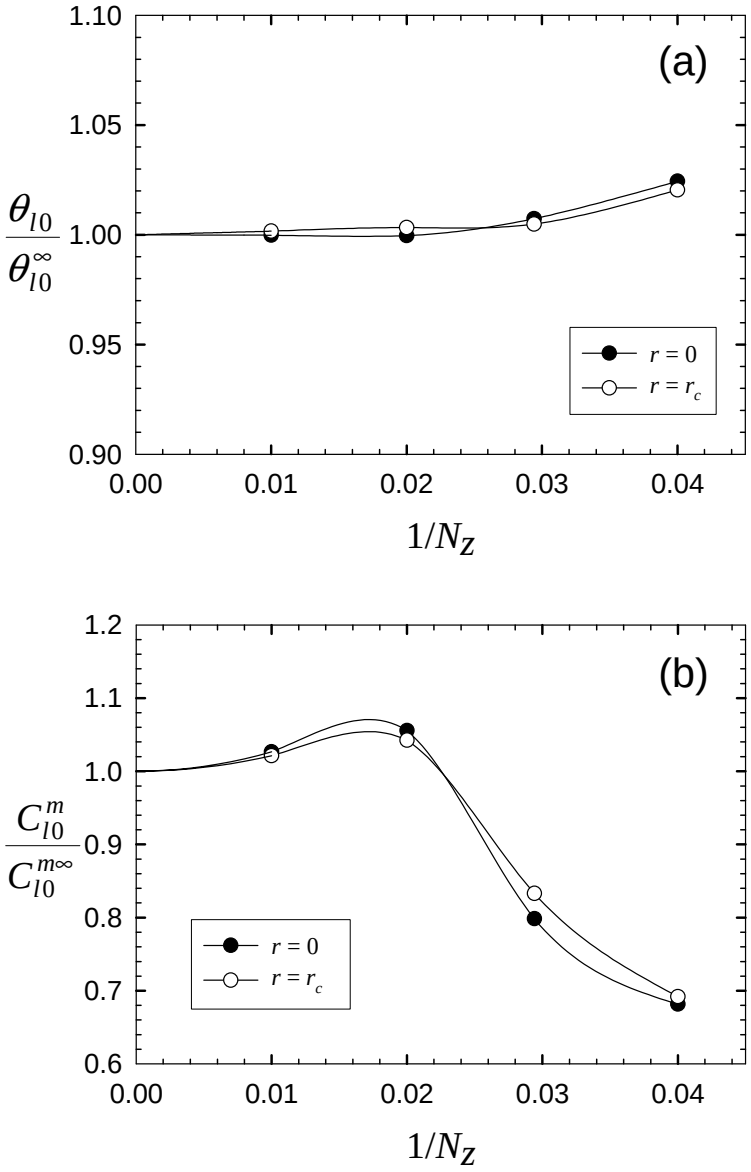


**Figura 3**





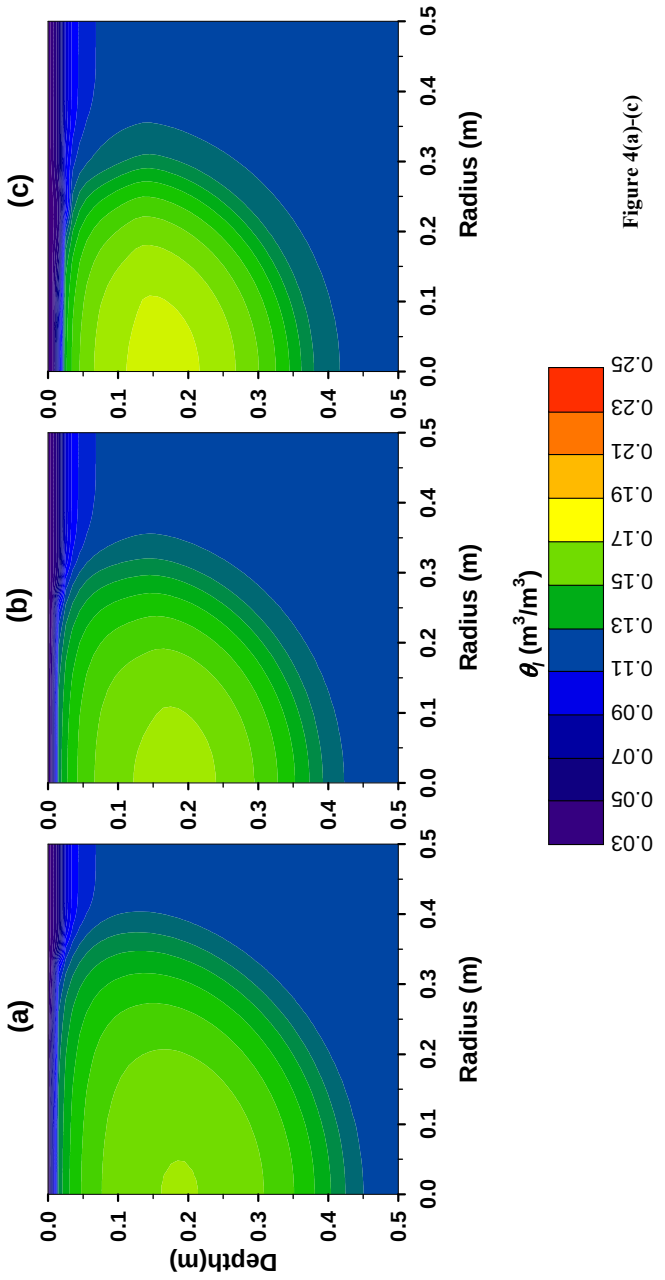


**Figure 4(a)-(c)**

UNIVERSITAT ROVIRA I VIRGILI
TRANSPORTE NO PASIVO DE COMPUESTOS ORGÁNICOS VOLÁTILES EN LA ZONA NO SATURADA.
Orlando Silva Rojas
ISBN: 978-84-690-7612-5 / DL: T.1217-2007



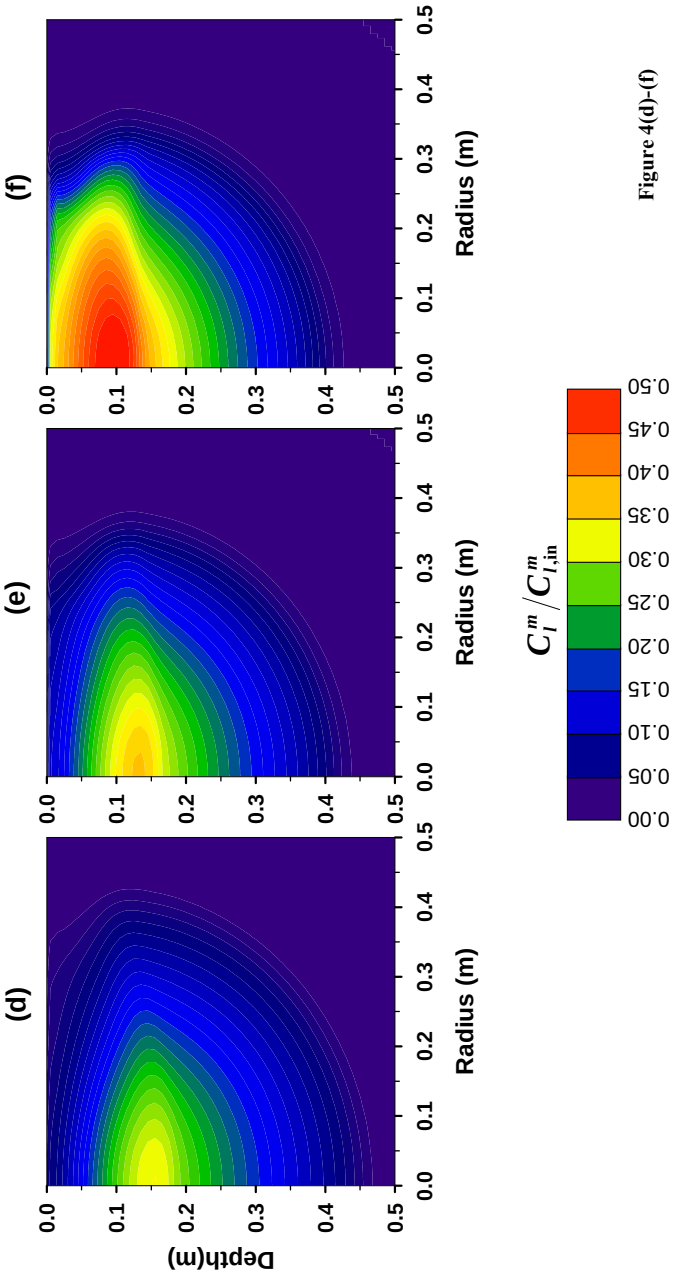


Figure 4(d)-(f)



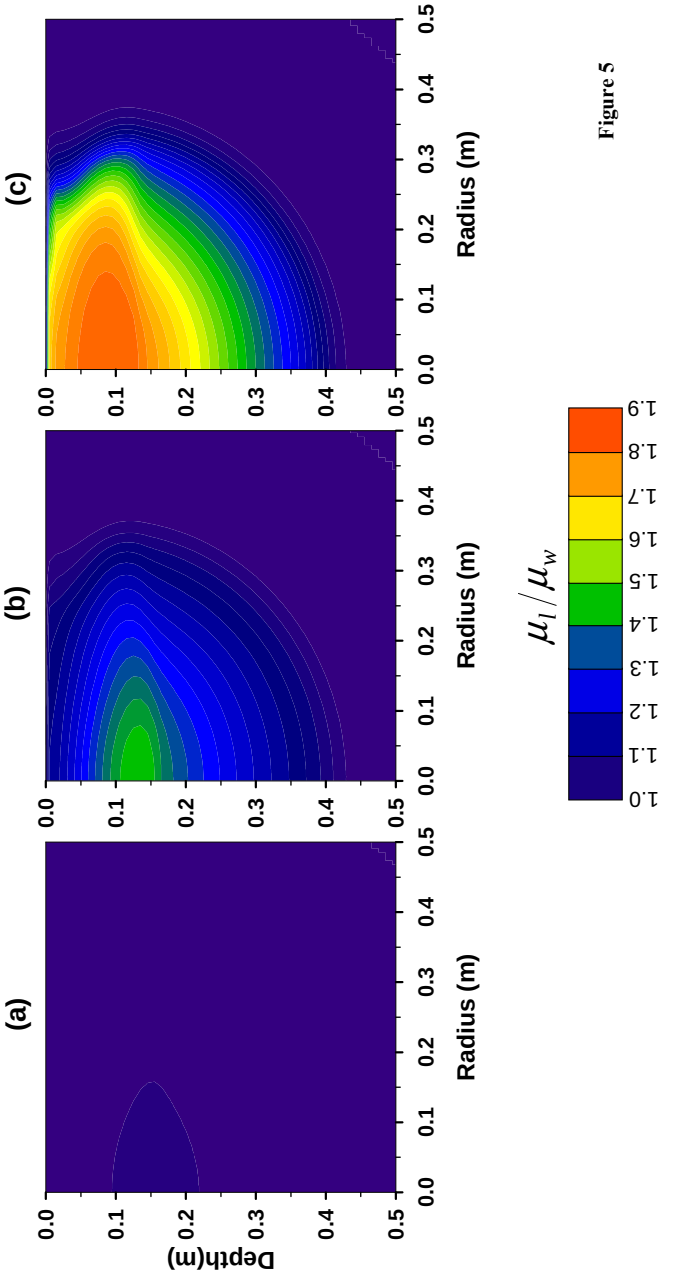


Figure 5

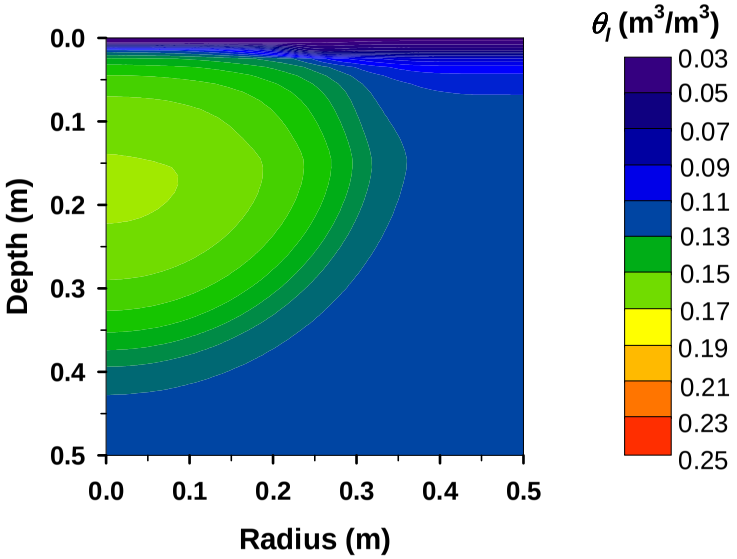


**Figure 6**



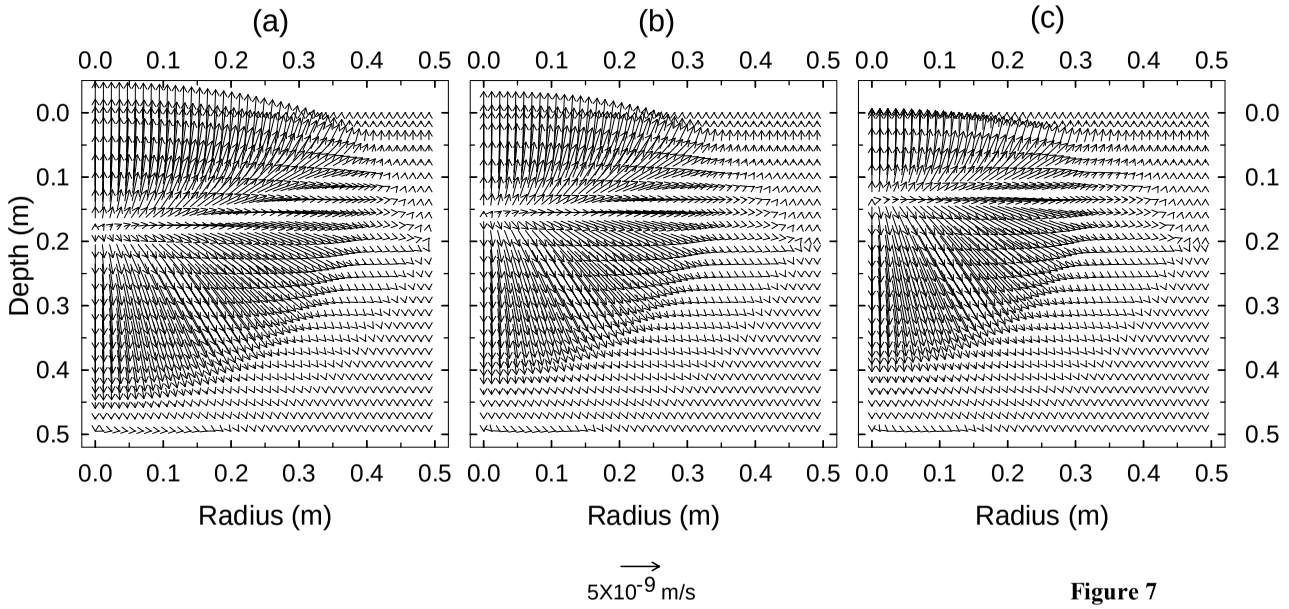


**Figure 7**

UNIVERSITAT ROVIRA I VIRGILI
TRANSPORTE NO PASIVO DE COMPUESTOS ORGÁNICOS VOLÁTILES EN LA ZONA NO SATURADA.
Orlando Silva Rojas
ISBN: 978-84-690-7612-5 / DL: T.1217-2007

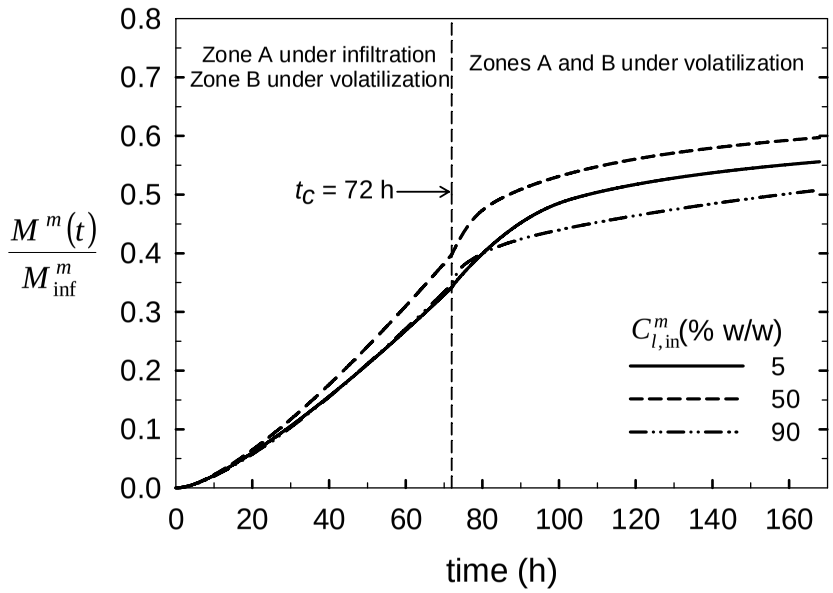


**Figure 8**



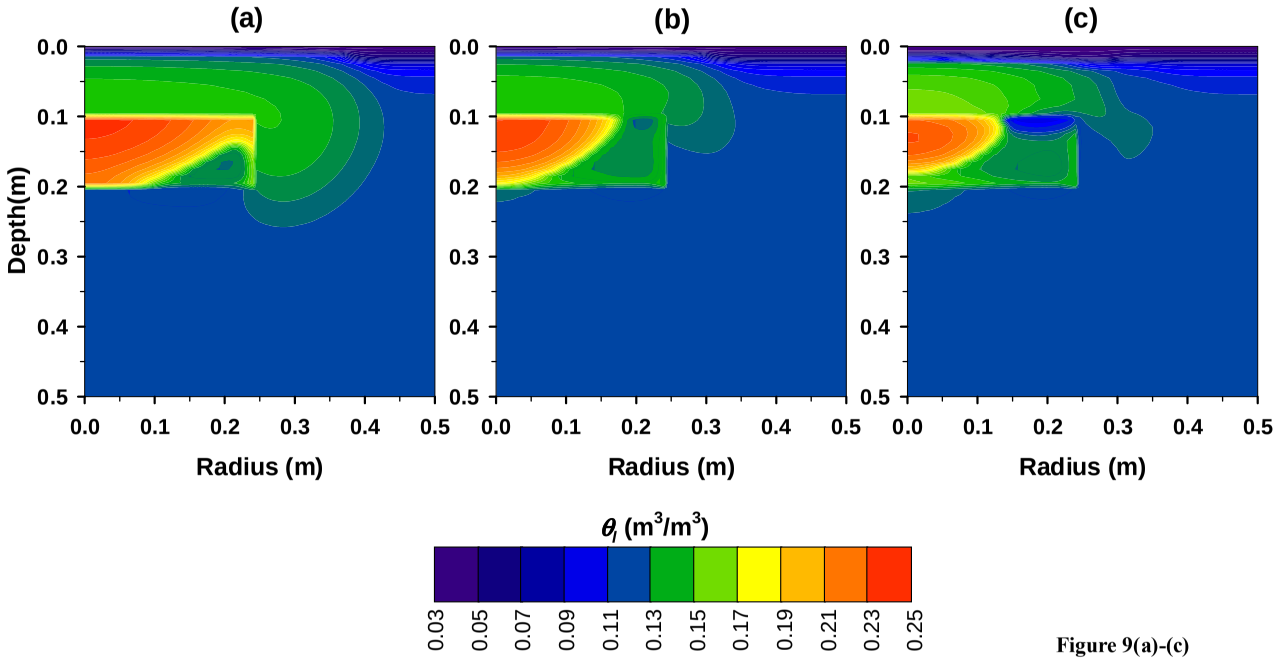


**Figure 9(a)-(c)**

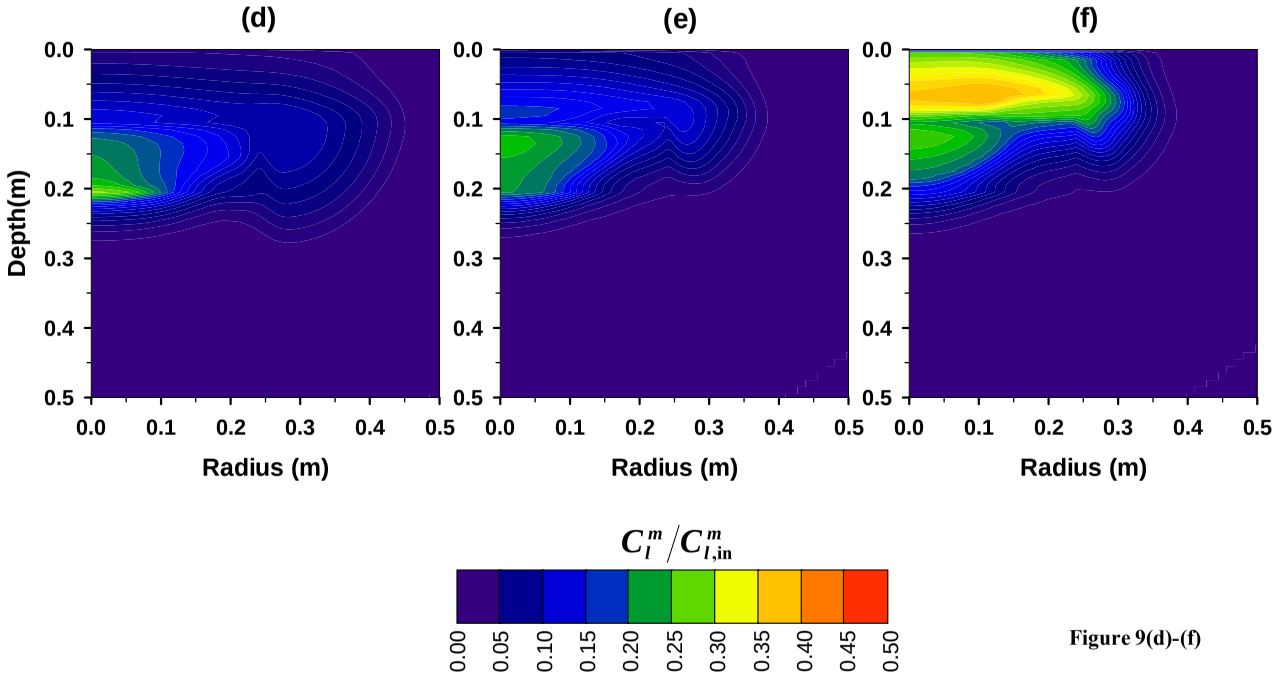


**Figure 9(d)-(f)**



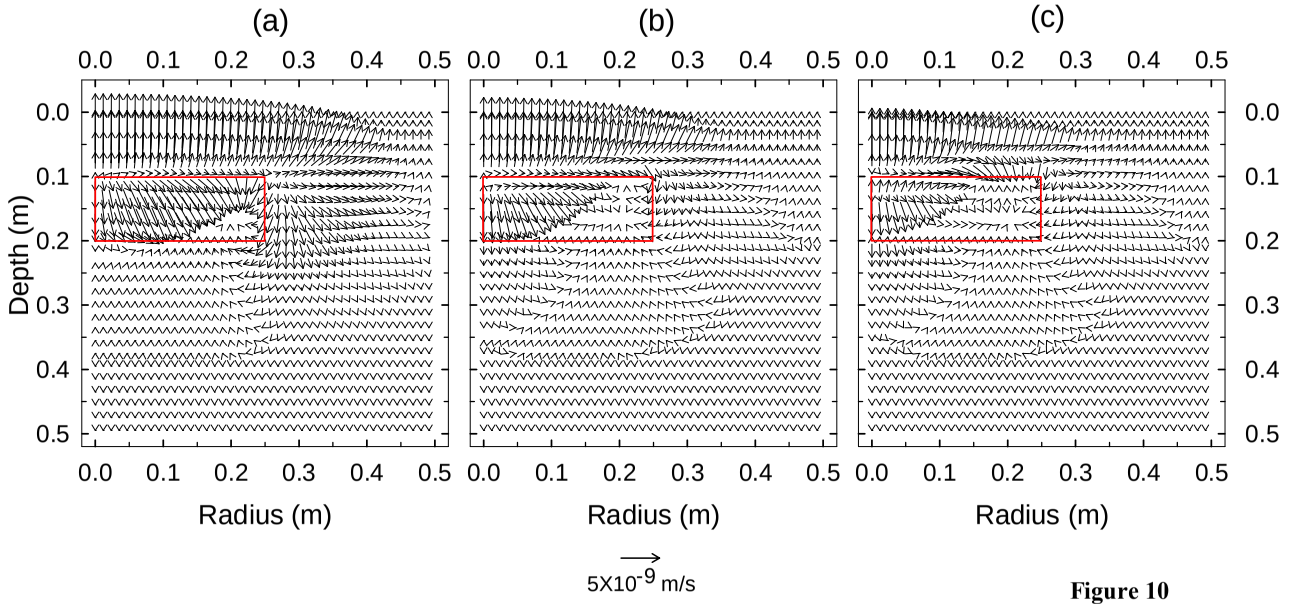


**Figure 10**

UNIVERSITAT ROVIRA I VIRGILI
TRANSPORTE NO PASIVO DE COMPUESTOS ORGÁNICOS VOLÁTILES EN LA ZONA NO SATURADA.
Orlando Silva Rojas
ISBN: 978-84-690-7612-5 / DL: T.1217-2007



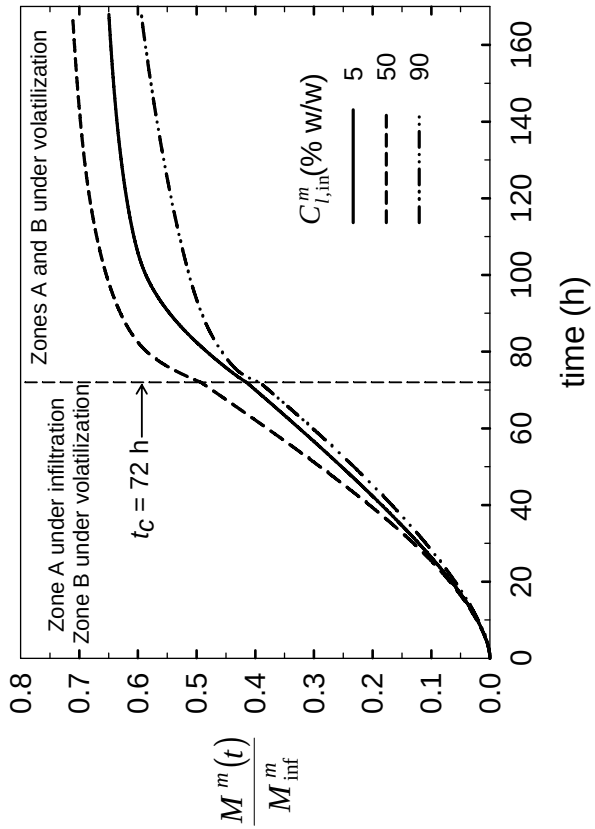


**Figure 11**



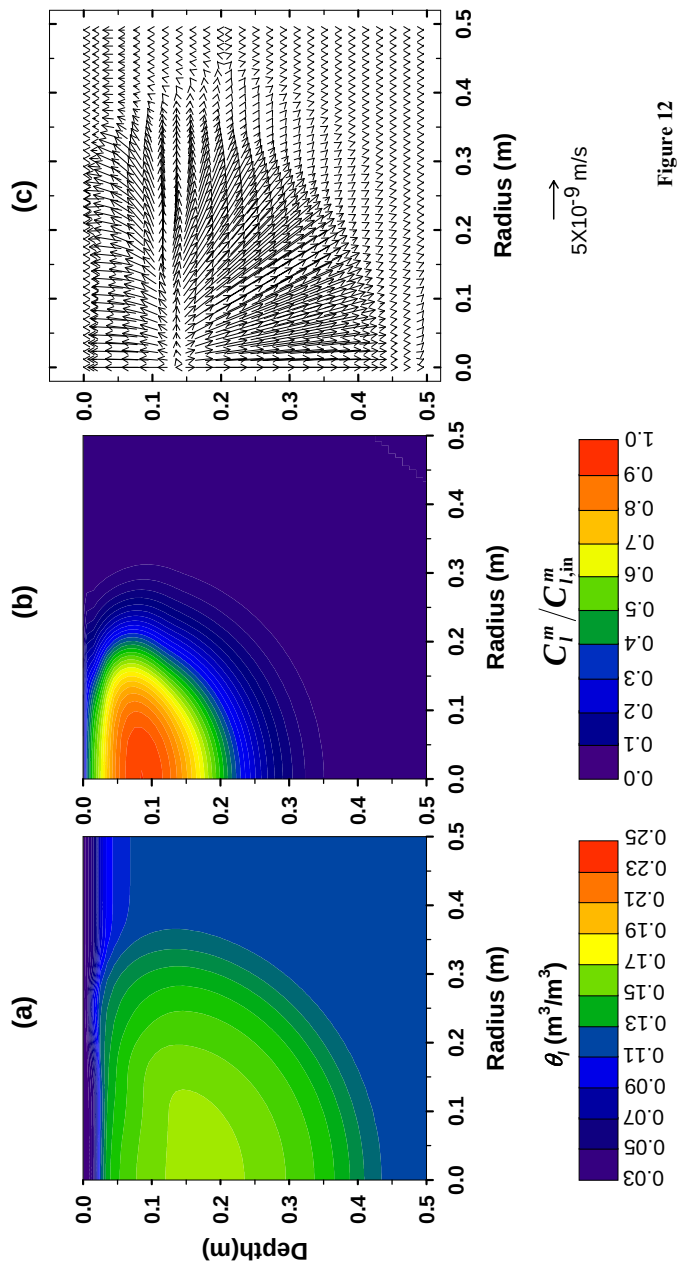


**Figure 12**

UNIVERSITAT ROVIRA I VIRGILI
TRANSPORTE NO PASIVO DE COMPUESTOS ORGÁNICOS VOLÁTILES EN LA ZONA NO SATURADA.
Orlando Silva Rojas
ISBN: 978-84-690-7612-5 / DL: T.1217-2007

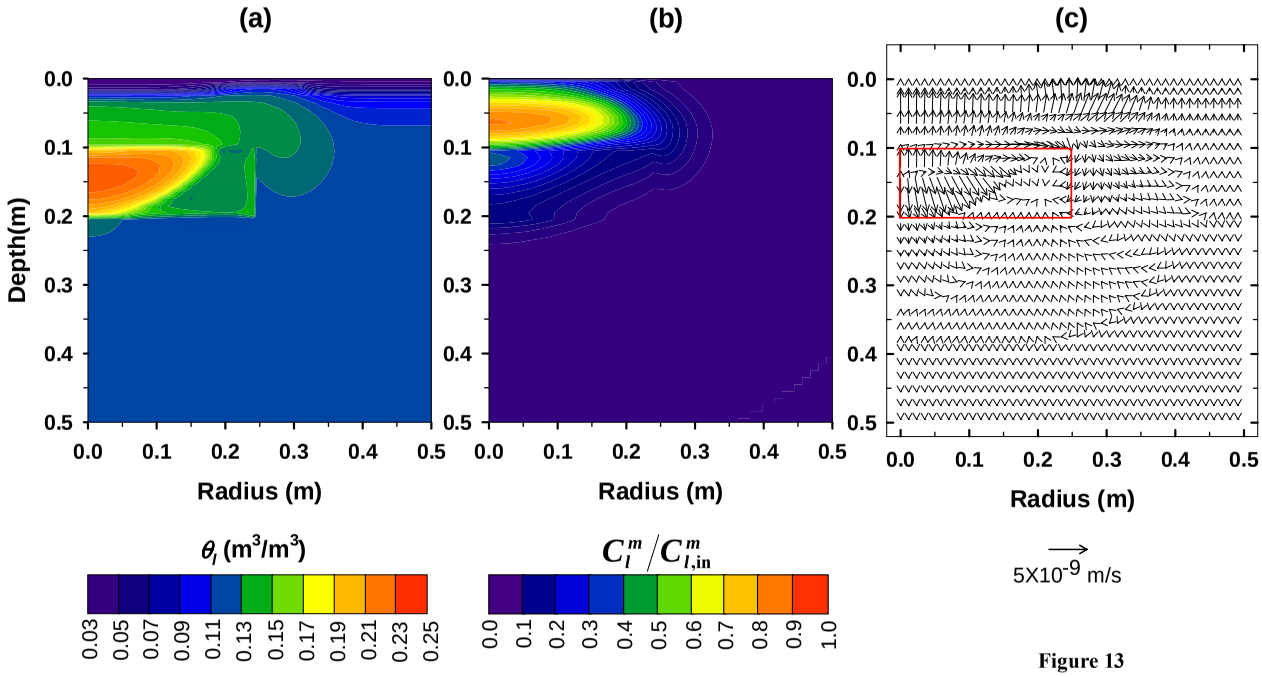


**Figure 13**